Department of Precision and Microsystems Engineering

Design of a Setup for Modal Testing of Micro-Cantilevers Immersed in Liquid

ing. B. van den Brink

Report no	:	2017.059
Coach	:	dr. ir. F. Alijani, dr. M.K. Ghatkesar
Professor	:	prof. dr. P.G. Steeneken
Specialisation	:	Dynamics of Micro and Nanosystems
Type of report	:	Master Thesis
Date	:	4 December 2017

TU Delft

Design of a Setup for Modal Testing of Micro-Cantilevers Immersed in Liquid

by

ing. B. van den Brink

to obtain the degree of Master of Science
at the Delft University of Technology,
to be defended publicly on Monday 4 December, 2017 at 15:00.

Student number:	4332008	
Project duration:	September 1, 2016 – December 4, 2017	
Thesis committee:	prof. dr. P.G. Steeneken,	TU Delft, Chair
	dr. ir. F. Alijani,	TU Delft, Supervisor
	dr. M.K. Ghatkesar,	TU Delft, Supervisor
	dr. ir. J.F.L. Goosen,	TU Delft, External expert

An electronic version of this thesis is available at `http://repository.tudelft.nl/`.

TU Delft

Abstract

To facilitate research on the dynamics of micro-cantilevers immersed in liquid, a modal test setup was designed. Modal testing is a powerful form of dynamic testing whereby the system's natural frequencies, modal masses, modal damping ratios, mode shapes, and weight of each of these modes at a certain frequency are determined. Micro-cantilever resonators are often used for sensing applications, where information is extrapolated from the change in dynamical behavior. Such systems are used in liquid environments to characterize the fluid density and viscosity, to measure the mass and stiffness of particles suspended in this liquid, and to image biological samples using atomic force microscopy. The designed setup employs piezoelectric base actuation to excite the cantilevers, of which the response is measured in vacuum, air, and water. A clean and spurious free response is achieved in a bandwidth ranging from 20 kHz to 500 kHz in vacuum and air, and a bandwidth ranging from 50 kHz to 500 kHz in water.

Preface

After one and a half to two years, this journey has finally come to an end. It was a great experience to delve in the micro-scale world, fabricate my own setup, and to discover the mysteries of modal testing and non-linear dynamics. I could not have done this without the support of my supervisors Farbod Alijani and Murali Ghatkesar. Next to my supervisors I wish to thank all my office mates, the people from the dynamics group, the guys from Taylor, and the technical support of PME. In particular I wish to thank Olivier, Bas, Joep and Raoul for making my years at PME awesome. Finally I wish to thank my parents, sister, and girlfriend Laura, for their endless support.

ing. B. van den Brink
Delft, November 2017

Contents

List of Figures

List of Tables

1 Introduction

During the sixties the first Integrated Circuits (IC) began to emerge, opening the doors to the digital revolution. The ICs are made from silicon wafers. Parts of these wafers are treated with a special process which enables the material to conduct electrical current. Thus, making the fabrication of electrical circuits on the micro-scale a reality. Soon people started to realize that, using the same fabrication methods, not only electrical components could be made at the micro-scale, but also mechanical, fluidic and optical components. This led to the research and development of a wide variety of microsystems. At first, this research was heavily focused on fabrication methods, but slowly, as fabrication methods were established, research shifted to improving the functionality and performance of these devices.

At the micro-scale other force types are dominant compared to those at the macro-scale. The contribution of surface and interface effects, such as surface tension and electrostatics, start dominating over volumetric dependent phenomena, such as inertia and magnetism. Also, the coupling between energy domains (mechanical, electrical, thermal, etc.) at these length scales is very high[4]. This greatly changes the dynamics compared to the macro-scale systems, and introduces new sources of nonlinear behavior[5]. Fluidic damping, even from air, has a considerable effect on the dynamics of the system[6].

Mechanical resonance is among the physical principles exploited in microsystem sensors. These sensors extrapolate information from the change in dynamical behavior of micro mechanical resonating structure. However, to facilitate research on the dynamics of these microsystems, proper test instrumentation is a necessity. Experimental research provides the dynamic characteristics of a system in practice, which in turn could be used for the verification and validation of theoretical models for example. Modal testing is the form of dynamic testing that is used for this purpose, whereby the system's natural frequencies, modal masses, modal damping ratios, mode shapes, and weight of each of these modes at a certain frequency are determined. These dynamic characteristics are used to: understand how a structure behaves under operational conditions, validate and update theoretical models, and speed up durability calculations.

The dynamic characteristics obtained from theoretical models are based on certain assumptions of boundary conditions, dimensions, material properties, and damping present in the system. In practice, these parameters might deviate due to the fabrication process of the materials and components, or change during the lifetime of the system. In addition, certain material properties might simply be unavailable during the modeling. Therefore, the need to characterize system dynamics in practice is of importance, particularly when dealing with highly complex systems. The exhaustiveness of a modal test can be varied depending on the complexity of the system, and the desired accuracy of the data acquired.

One area of research in the field of microsystem engineering studies the dynamics of these systems in liquids. Micro mechanical instruments can be used to probe or inspect biological samples in their natural environment, or to determine the fluidic and rheological properties of the liquid in which they are immersed (e.g. viscosity and density). Submerging a structure in liquid has substantial effects on its dynamic characteristics. During the design of microsystems operating in liquid, a proper understanding of the fluid-structure interaction is necessary, especially for sensing applications, where a high accuracy is essential. Micro-cantilevers are among the devices used for sensing applications. Due to their simple geometry, their theoretical dynamic behavior can be described analytically and numerically with relative ease, making them a popular choice as micro-mechanical resonators. This thesis investigates the different aspects involved in the design of a modal testing device for micro-cantilevers submerged in liquid.

1.1. Applications

The development of a modal test setup for the analysis of the dynamics of micro-cantilevers in liquids has a variety of applications. Research has indicated that when higher-order modes are taken into account, the resolution of Atomic Force Microscopes (AFM) increases [7–16]. Modal testing could aid the research and design of AFM cantilevers by, e.g., characterizing the dynamic behavior of the tip sample interaction[8–10, 13]. Another example where modal testing could be applied to micro-cantilevers in liquid is during mass sensing. Here the mass of a particle, or an organism, in the liquid is determined by observing the frequency shift caused by particle, or organism, adhering to the resonator. Research indicates that the sensitivity of such measurements can be increased, when higher-order modes are taken into account[17–19]. Similarly the sensitivity of micro-scale rheology instrumentation could be increased by taking higher-order modes into account[20–23]. This field of research concerns itself with the flow of liquids, and the relating properties (density, viscosity etc.).

1.2. Assignment Description

The goal of this project is to design, and build, a test setup with which the dynamic behavior of a micro-cantilevers in liquid can be determined. The influence of the test setup itself on the dynamic behavior should be minimized for a proper representation of the system in practice. During the design, the measurement system will be restricted to the Polytec Micro system Analyzer (MSA), which is already present at the department. The microsystems under test will be restricted to AFM micro-cantilevers. Further details about the constraints and scope of the project can be found in appendix A.

1.2.1. Problem Definition

The problem identified in literature, as further discussed in chapter 2, can be defined as:

- A suitable actuation method for modal testing in liquid has still to be selected
- Influence of vibrations from the setup on the dynamics of the cantilever is still unclear
- Basic forms[1] of vibration testing and modal analysis are currently used to investigate the dynamics of micro-cantilevers in liquid

1.2.2. Research Question

The research question driving this project is defined as: *How can modal testing of micro-cantilevers immersed in liquid be performed properly[2]?*

To answer this question, the following challenges are encountered:

- How to detect the vibration response of the cantilever with the LDV when the cantilever is in chamber filled with fluid?
- How will the actuation of the cantilever be implemented in a liquid environment?
- How to mount the cantilever such that the energy transfer from the actuator to the sample is optimal?
- How can the influence of spurious vibrations from the test setup on the sample be minimized?
  - Environment chamber vibrations
  - Mounting vibrations
  - Liquid vibrations
  - Actuator vibrations

[1] These forms are described by Ewins [24] as levels and are found in appendix B.1
[2] Low coupling between setup vibrations and sample, low signal to noise, low influence on the dynamics of the system under test

1.3. Approach

To successfully design the test setup, first a literature review will be conducted in order to gain insight into the current condition of the research field. This literature review is done not only to get acquainted with the research already done in the field, but also to uncover new research opportunities.

Hereafter the concept phase will be initiated, in which conceptual designs will be generated and evaluated with back of the envelope calculations. From the concept, and with the knowledge obtained from the literature review, a detailed design will be made, and produced. To aid the design, next to the literature review, experiments in air will be done to gather experience with modal testing micro-cantilevers and modal analysis using the software package SDTools. Finally, the testing and validation of the setup will be preformed. During this last phase, several micro-cantilevers will be tested to demonstrate the capabilities of the setup.

1.4. Thesis Outline

First the elementary components of the setup will be discussed in chapter 2, including the literature available for each separate component. Hereafter the detailed design, the actuator models and the fabrication will be explained in chapter 3. The validation of the design and the obtained response of the tested micro-cantilevers will be discussed in chapter 4. The final conclusions and recommendations can be found in chapter 5. To reduce the length of the thesis, all introductory information about modal testing, fluid-structure interaction of microsystems, and acoustics, has been moved to appendix B, C, D respectively. For the interested reader, details about the project which could not be elaborated in the thesis itself have also been moved to the appendices. This includes the project confines formulated after the literature review, the morphological analysis done to aid the concept selection, further details taken into account during the design, and an additional frequency response curve not shown in chapter 4. This information can be found in appendix A, E, F, G respectively.

2

Elementary Components

This chapter attempts to give a broad overview of the elementary components of a modal test setup for liquid immersed microsystems in general, including micro-cantilevers, and discusses the literature on this subject. The elementary components of a model test setup for microsystems immersed in liquid, can be identified as: the actuator that excites the microsystem, the mounting the microsystem is attached to, the environment in which the microsystem is immersed, and the measurement system to measure the vibrations of the microsystem. A labeled schematic of a test setup is including these components shown in figure 2.1. An evaluation to decide which components are critical, and in which areas more research is necessary, has to be done for substantiated decisions during the design. Lin *et al.* [6] did an extensive literature review on structural dynamics of microsystems, including vibration testing, in 2006 which included excitation and measurement methods.

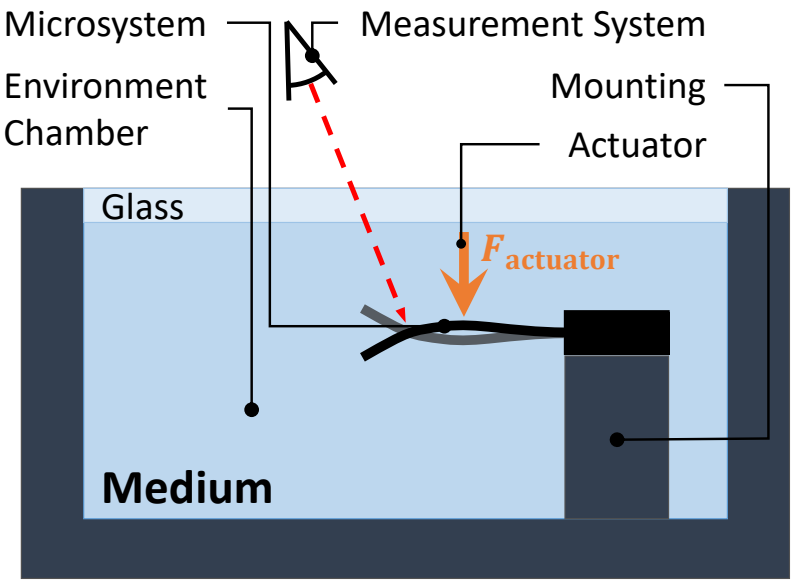

Figure 2.1: Schematic representation of a setup for modal testing a structure immersed in a medium

2.1. Actuator

For proper excitation of the micro-structure the influence of the actuator on the dynamic behavior of the microsystem and its fluid-structure interaction should be negligible. In case of experimental modal analysis the applied force should be well defined through direct measurement, or through the measurement of the actuator input and the use of an highly accurate model of the force the actuator applies with respect to a

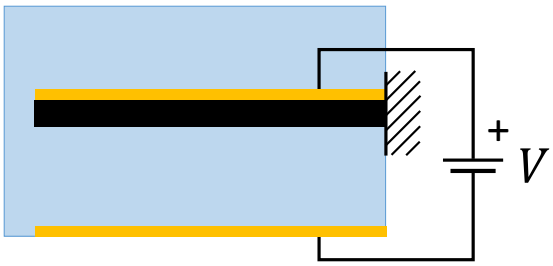

(a) Electrostatic excitation

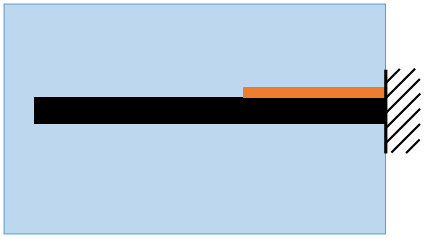

(b) Integrated excitation

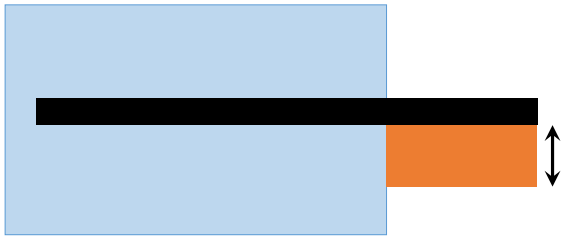

(c) Piezoelectric base excitation

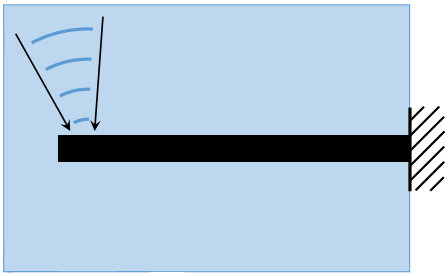

(d) Acoustic excitation

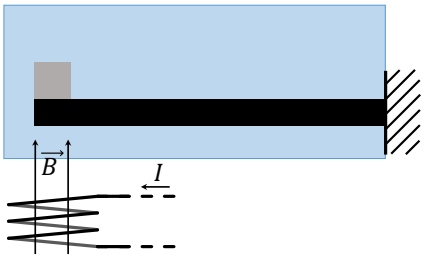

(e) Magnetic excitation

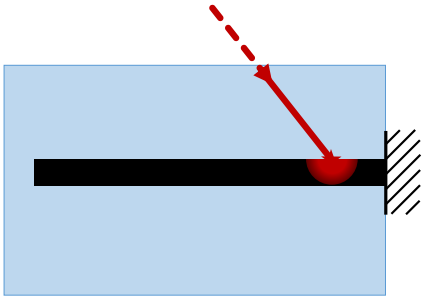

(f) Photo-thermal excitation

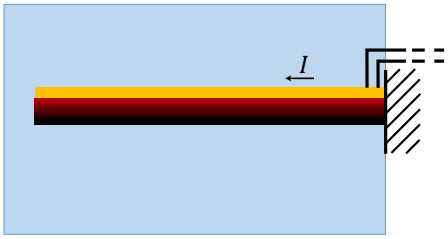

(g) Electro-thermal excitation

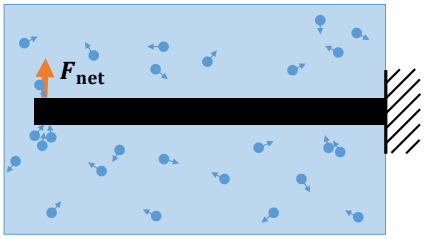

(h) Brownian excitation

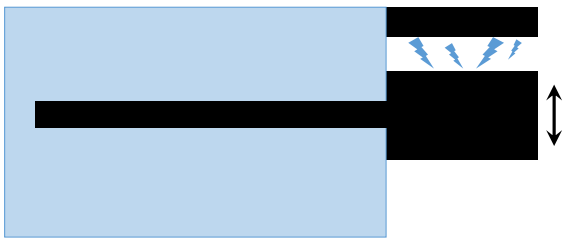

(i) Electric discharge excitation

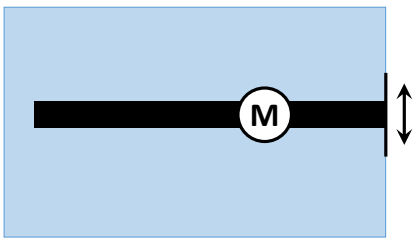

(j) Operational excitation

Figure 2.2: Actuation methods

given input. In the case of operational modal analysis[1] the (stochastic) applied force should be distributed in such a way that it can be considered a MDOF excitation. A well defined, or measured, point force would be the easiest to process during analysis and a distributed stochastic force the most difficult, because the exact distribution is not known in general. Due to the high viscous damping from the liquid, the vibrations transmitted from the point of excitation throughout the structure diminish rapidly and become unobservable at a certain point. This range determines the size of the area that can be used for modal analysis. Also, the actuator should have an appropriate bandwidth to measure the modes, or frequencies, of interest.

Xu *et al.* [25] compared the main excitation methods used for the excitation of AFM cantilevers in liquids (Piezoelectric base, Brownian noise, and Magnetic) and concluded that magnetic actuation showed the highest potential for the actuation of the first mode. Later Penedo *et al.* [26] evaluated methods for the excitation of higher order modes in AFM cantilevers in liquids (Magnetostriction, Magnetic torque, and Photo-thermal) and concluded that magnetostrictive actuation showed the highest potential. These assessments were made with the requirements for atomic force microscopy of biological samples in mind. However, those experiments were less concerned with exact measurement of the excitation force needed to determine the weight factors of the modes. The research does give great insight into the different forms of excitation however. Here follows an assessment of the different excitation methods for modal testing of microsystems in liquid, based on previous research.

Electrostatic excitation is achieved by integrating an electrode into the structure or by coating the structure with a conductive layer [27], as shown in figure 2.2a. A voltage is induced between the electrode and a counter-electrode attached to the environment chamber, resulting in an electrostatic force on the structure. This method of excitation is rather straightforward, however the added mass and stiffness influence the dynamics of the system, and accurate data of the amplitude and distribution of the applied electrostatic force is difficult to obtain.

Integrated excitation is based on the application of patches of "smart material" integrated in the microsystem, as shown in figure 2.2b. These patches consist of a film of piezoelectric material [28], or magnetostrictive material [29]. These patches are actuated by applying an electric potential or a magnetic field respectively. The advantage of this method is the precise location of the force applied and the short distance between the actuator and the structure. The application of such patches influences the mass and stiffness of the system however. The process of applying these materials on the system is also rather intensive, compared to the application of a thin-film of conductive material.

Piezoelectric base excitation, also known as acoustic base excitation, is a excitation method often employed in the case of modal testing of microsystem in vacuum or gaseous environments [30]. A microsystem is attached either directly, or by a holder, to a piezoelectric element, as shown in figure 2.2c. In this way the the base of the microsystem is excited, causing vibrations in the structure. An other option is to use the piezoelectric element to introduce a shock to the base of the microsystem, in literature referred to as bulk acoustic wave excitation [31]. The advantage of this technique is that the microsystem in question does not have to be altered in any way. Also, the effect of the actuator on the dynamics of the system is negligible in vacuum and gaseous environment.

Difficulties with this excitation method arose when applied in liquid environments in the form of spurious peaks, also known as "the forest of peaks" [32]. An other concern is fluid-borne excitation of the microsystem by vibration of the microsystem holder in the liquid, causing acoustic waves in the liquid [25] of which the forcing on the structure is difficult to model. Efforts have been made to understand and reduce these spurious peaks [33–35], which some researchers contributed to the design of the liquid environment, and others to the microsystem holder.

It is important to note that, as with the integrated smart material actuation, other materials apart from piezoelectric materials, such as magnetostrictive materials for instance, could be used for base excitation. In addition, the movement of the base can be measured with relative ease, which could be used to compensate for some of the actuator dynamics during analysis by analyzing transmissibility.

Acoustic excitation is accomplished by sending acoustic waves through the liquid to the microsystem, transferring the momentum of the acoustic radiation pressure to the structure, as shown in figure 2.2d. The acoustic wave is generated by a piezoelectric transducer and focused to improve performance [36].

[1] Appendix B

No alteration of the microsystem is necessary to facilitate this form of excitation, however the acoustic vibrations might excite resonances in the liquid cell. It is also challenging to measure or deduce the applied force with this excitation method, especially since the spot size varies with frequency with $d_{\text{spot}} \approx \frac{c}{\Phi f}$ [37], where d_{spot} denotes the spot size diameter, c denotes the speed of sound, Φ denotes the total angular beam spread, and f the wave frequency.

Magnetic excitation is achieved by attaching a magnetic particle or thin-film to the microsystem. The microsystem is subsequently excited by applying a oscillating magnetic field [38, 39], as shown in figure 2.2e. Depending on the orientation of the magnetic field and the magnetized particle or thin-film, the excitation is either flexural or torsional (also known as MAC mode [26]). Magnetic excitation is a popular excitation method for cantilevers in liquids [25] due to the difficulties experienced with piezoelectric base excitation in liquids. The advantage of magnetic actuation is the limited influence the excitation has on the fluid. It does influence the microsystem itself by adding mass and stiffness in the form of a magnetic particle or layer though. Also, the limited bandwidth might make excitation of higher order modes rather challenging [26].

Photo-thermal excitation method makes use of a laser beam to locally heat the structure, as shown in figure 2.2f, inducing vibrations [40–42]. These induced vibrations can be caused by different phenomena. First, the momentum transfer from the photons of the laser beam to the structure will result in vibrations. The second effect is related to the temperature gradients induced by local heating due to the laser. Often the microsystem is also coated with a metallic layer causing bi-morph bending, which is caused by the different coefficients of thermal expansion. The advantage of this method is the high bandwidth compared to magnetic excitation. The applied force is difficult to deduce accurately however, and even though application of a metallic thin film might not be requisite for successful excitation, the effect of local heating might have significant effects on the dynamics of the microsystem.

Electro-thermal excitation is caused by oscillated joule heating of integrated circuits in the microsystem [43], as shown in figure 2.2g. The thermal expansion of certain parts of the system induces vibrations. This technique requires an integrated circuit, which together with the thermal effects caused by the heating, influence the system dynamics.

Brownian excitation is inherent to the thermal bath of the fluid in which the microsystem is submerged[2]. In figure 2.2h, a schematic representation of the excitation method is shown. The vibrations caused by Brownian forcing, or thermal noise, is often employed for the calibration of atomic force microscopes [44–46]. Because this excitation force is inherent to the fluid itself it does not alter the dynamics of the system and fluid-structure interaction in any way. The average spectrum of Brownian forcing can give insight to the dynamics of the microsystem using operational modal analysis techniques. This takes a significant amount of time compared to experimental modal analysis though, since the magnitude of the response is proportional to $\frac{1}{\sqrt{N}}$, where N is the amount of data samples. Due to the stochastic nature of the force, it is improbable that the applied force can be measured in time or frequency domain with current technology, which makes this excitation technique a poor candidate for pure experimental modal analysis. Modal analysis can still be preformed using operational modal analysis techniques however. Prior knowledge of the system's stochastic behavior (i.e. models), as is the case with Brownian excitation, will ease the process of operational modal analysis and increase its accuracy.

Electric discharge excitation is a transient excitation method in which a microsystem holder, on which the microsystem is fixed, is excited by an electric spark [47], as shown in figure 2.2i. This introduces shock in the holder with a wide frequency band. Similar to piezoelectric base excitation, the dynamics of the holder could affect the dynamics of the structure.

Operational excitation , shown in figure 2.2j, is a technique in which the actuators of the microsystem itself are used to excite the structure [48], which limits this technique to microsystems with built-in actuation. Depending on the microsystem the determination of the applied force might be difficult.

2.2. Mounting

Little research has been done on the way the microsystem is attached to the holder. In the case of modal analysis of microsystems in vacuum or air, the performance difference between wax and superglue was compared

[2] Appendix C

[30]. In contrary to the wax, the superglue did not affect the dynamics of the system. Other options, such as clamping for example, and the compatibility with the liquid environment have not been taken into account.

2.3. Liquid Environment

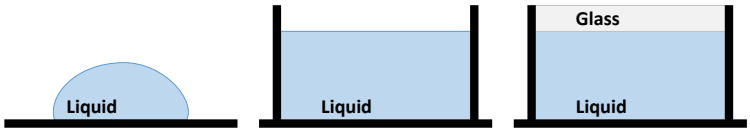

(a) Droplet (b) Open liquid cell (c) Closed liquid cell

Figure 2.3: Liquid environment types

The common liquid environments in use can be divided into three different types: the bare droplet, the open liquid cell and the closed liquid cell. The most basic of the three is the bare droplet, shown in figure 2.3a. Due to the size of the microsystems under test, a simple droplet can serve as a liquid environment. A droplet evaporates easily though, which is a drawback of this liquid environment type. Evaporation can change the composition of the liquid in case of emulsions or solutions. An other common liquid environment is the open liquid cell, shown in figure 2.3b. These cells are commercially available, although a Petri dish is a common substitute. This liquid environment allows for a larger liquid bath, which reduces evaporation issues. The most advanced liquid environment is the closed liquid cell, shown in figure 2.3c. This cell is also commercially available and prevents evaporation by fully enclosing the liquid. The functionality of both the open- and closed liquid cells can be extended such that, for example the liquid temperature or pressure, can be controlled.

During research on the applications of the dynamic mode of atomic force microscopes in a liquid environments, the influence of the liquid cell design on the dynamic behavior of the microsystem was observed [32]. Allegedly the vibrating microsystem and holder (attached to a piezoelectric element) excited the dynamic response of the liquid cell. Further research was done on a commercial liquid cell by comparing the response of different cantilevers, which concluded that the spurious peaks in the vibration response mentioned earlier can be contributed to the liquid cell [49]. Other research refutes this however, and contributes the effect to the dynamic response of the holder of the piezoelectric excitation device [50].

Much remains unclear and further investigation is necessary to successfully design a proper liquid environment, taking the dynamic response and acoustics into account.

2.4. Measurement System

Measurement systems can be generalized into two categories. The first category are laser based systems, such as optical lever detection (common in atomic force microscopes), Laser Doppler Vibrometry (LDV), Electronic speckle pattern interferometry (ESPI), and classical interferometry with either continuous or stroboscopic illumination. These techniques are most suitable for out-of-plane vibration measurement. The second category is based on CCD camera image processing, which is suitable to measure in-plane vibrations and can, in some cases, also measure out-of-plane vibrations. These techniques are less commonly employed and much is still in research and development. Examples are the Computer Microvision Systems (CMS) developed by MIT [51], and the development of an in-plane displacement detection algorithm by Kokorian *et al.* [52].

Due to the availability of a LDV, it has been chosen to restrict the measurement system to the use of this device for this project. This restricts the research to out-of-plane vibrations.

An LDV is used to measure the vibrations of structures without introduction of added inertia. This is especially important for small systems, since the mass of the transducer, compared to the test structure, would alter the dynamics of the test structure in a significant way. In addition, the LDV provides a way to measure structures that are difficult to access or where it is challenging to attach a sensor to the structure.

An LDV is essentially a double beam interferometer that utilizes the frequency shift between the two beams, generated by the Doppler effect, to extract the velocity of the vibrating structure. The direction of this velocity is extracted by adding a Bragg cell to one of the beams, which shifts the frequency of the light from that beam. This is done to ensure that the frequency difference between the two beams is always pos-

itive, even if the frequency shift by the Doppler effect is negative. In practice this ensures that the intensity shift, due to the Doppler effect, detected by the photocell is non-symmetric.

Since the LDV supplies information from the double beam interferometer as well as the Doppler frequency shift, it can be used for displacement and velocity measurement alike. Displacement demodulation is better suited for low frequency measurements and velocity demodulation is better for higher frequencies.

2.5. Concept Selection

To minimize the bias when selecting the components for the conceptual design, a morphological analysis is done. The measurement system is left out of this analysis, since the available LDV at the department already meets the requirements. The environment chamber is also left out of the analysis, since the chamber will be designed in such a way that, next to various liquids, different kinds of gasses can be used at pressures varying from atmospheric to a vacuum level of 10^{-3} mbar[3] [53]. As a consequence, the environment chamber is restricted to a closed liquid cell.

The factors that are taking into account during the selection of the mounting principle are: the damping the mounting imposes, the robustness of the joint, the fabrication difficulty, the ease of use, and the estimated cost. These selection criteria where given a weighting factor and graded by the members of the project to get as close as possible to an unbiased selection. As a result gluing was selected a mounting method (tab. 2.2), with clamping as a close second. Later in the project however, clamping is selected as mounting method due to unsatisfying experiences with gluing, and working principle, which complements a design where the mounting is integrated in the wall of the environment chamber as will be discussed in chapter 3.2.

The same procedure is used during the actuator selection (tab. 2.1), which is done taking into account: the actuator influence on the dynamics of the system (e.g. by adding mass or heating up the system), supported by back-of-the-envelope calculations and values from literature, the maximum excitation bandwidth and amplitude range, supported by values found in literature, the fabrication difficulty, the difficulty of force estimation/detection, the ease of use and the estimated cost. From this analysis, piezoelectric base excitation appears to have the most potential.

Table 2.1: Morphological analysis of the actuator concepts. Each criteria is graded for each concept with a number between 1 and 10, with 10 indicating the best performance.

Weight	22%	30%	17%	8%	12%	7%	5%	100%
Actuation	**Influence on dynamics**	**Excitation bandwidth**	**Amplitude range**	**Fabrication**	**Force detection**	**Operation**	**Cost**	**Total**
Electrostatic	4.67	8.00	7.67	5.00	8.33	8.67	7.00	7.01
Integrated piezoelectric	4.67	9.67	6.67	4.67	9.00	7.67	3.67	7.16
Magnetostrictive	5.67	6.67	5.33	6.33	7.33	5.33	3.67	6.04
Piezoelectric base	8.67	9.33	7.67	6.67	8.00	8.33	8.67	8.43
Magnetic	4.33	6.67	7.00	6.00	7.33	8.00	5.33	6.26
Photo-thermal	7.00	7.33	4.00	5.67	5.00	6.33	5.67	6.14
Electro-thermal	2.33	3.33	4.00	5.67	6.33	6.67	3.00	3.98
Shape memory alloy	1.00	1.00	4.33	1.67	6.00	5.00	1.67	2.49

[3] Appendix F.2

Table 2.2: Morphological analysis of the mounting concepts. Each criteria is graded for each concept with a number between 1 and 10, with 10 indicating the best performance.

Weight	25%	35%	10%	18%	13%	100%
Mounting	**Damping**	**Robustness**	**Fabrication**	**Operation**	**Cost**	**Total**
Glue	7.50	10.00	6.00	4.50	8.00	7.76
Double sided tape	4.50	6.00	7.50	5.00	10.00	6.10
Clay	5.00	5.50	8.00	8.00	8.50	6.44
Wringing	7.50	3.50	6.00	4.50	6.00	5.24
Spring	8.00	6.00	7.00	8.50	6.50	7.10
Temperature preload	6.50	7.00	4.00	6.00	3.50	5.96

3

Setup Design and Fabrication

This chapter discusses the different aspects involved with the design of the modal test setup and its fabrication. A thorough understanding of the physical principles involved is necessary to make substantiated design choices.

3.1. Actuator Configurations

Fundamentally the design of a piezoelectric actuator for base excitation is similar to the design of an ultrasonic[1] transducer. Both use a piezoelectric element (piezo) to convert electrical power to mechanical vibrations and transmit these to a target body, i.e., the chip base. The application however, is slightly different. Ultrasonic transducers are used as an imaging device in various fields (e.g. non-destructive testing, medical ultrasound and SONAR) for instance, where a sensing transducer is used to monitor the echo of waves, originating from a emitting transducer, reflecting on structures and boundaries in the target body. Power ultrasonics (e.g. ultrasonic cleaning, ultrasonic welding and ultrasonic metal forming) is another application area of ultrasonic transducers, where high-intensity vibrations are induced to alter (e.g. cavitation) the target body. In both these cases, the emitting transducers are designed to be used at a relatively narrow frequency band. For optimal performance this frequency should be a resonance frequency of the transducer. This differs from the actuator for base excitation, which has to operate in a wide range of frequencies.

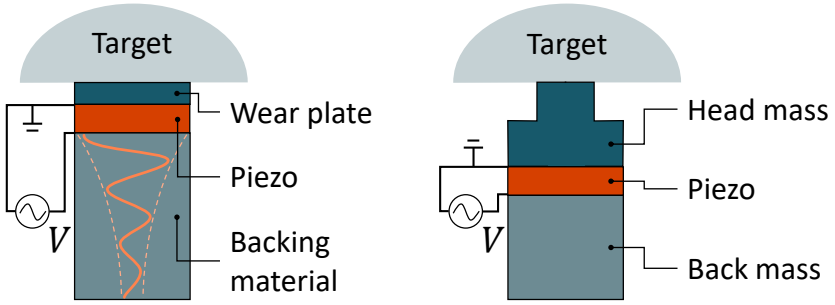

(a) Single element transducer (b) Langevin transducer

Figure 3.1: Basic ultrasonic transducer designs

Figure 3.1 shows the basic ultrasonic transducers types. The single element transducer (fig 3.1a) consist of a wear plate, the piezoelectric element and the backing material. The function of the backing material is to damp out the back-traveling vibrations, thus preventing an echo of the excitation signal to reach back to the piezo, and therefore also preventing standing waves, i.e. resonance. Usually the backing material is made from a particle filled composite, where the matrix material mainly contributes to the damping and the material of the particles is chosen in such a way that the acoustic impedance[2] of the backing material

[1] Although ultrasonic transducers typically operate at ultrasonic frequencies (>20 kHz), transducers operating at sonic or subsonic frequencies are commonly also referred to as ultrasonic transducers

[2] Appendix D

matches the impedance of the piezo. The advantage of this design is that the highest operating frequency (i.e. the first resonance frequency) depends solely on the dimensions of the wear plate and piezo. This design is disadvantageous at lower frequencies though. The necessary minimum length of the backing material increases rapidly with decreasing frequency, since the attenuation coefficient is proportional to the frequency squared[2]. This length determines the lowest operating frequency of the transducer.

The Langevin, or Tonpilz, transducer (fig 3.1b) consists of a head mass, the piezo and the back mass. The back mass acts as an inertial balance mass and will, in combination with the head mass, determine the amount of force which can be delivered to the target body. The first resonance frequency of the transducer is determined by the concatenation of all the components, which makes this design more fit for lower operating frequencies. The shape of the head mass usually depends on the application. Especially for power ultrasonics such as ultrasonic welding and ultrasonic cutting, the head mass is usually shaped in such a way that the force from the piezo is concentrated at the tip of the transducer, similar to the working principle of a needle. A shaped head mass is referred to as an acoustic horn, sonotrode, acoustic wave-guide or ultrasonic probe.

In both cases the wear plate and head mass of the transducers protect the piezo from scratching, and isolates the piezo from liquid, thereby protecting the piezo from short-circuiting. The material of the wear plate and head mass, if properly chosen, can ease the impedance mismatch of the piezo and the target body.

It is important to note that separating the piezo from the liquid is crucial in the design of a piezoelectric actuator. This introduces an extra component compared to designs aimed at gaseous environments or vacuum, where short-circuit protection is of less importance, due to the high electrical breakdown voltage of gasses compared to liquids. The introduction of this component and the way it is integrated in the environment chamber increases the complexity of the design.

Due to the required bandwidth (1 kHz to 1000 kHz) of the actuator for base excitation, the Langevin transducer design is preferred. A stepped acoustic horn will be taken as head mass to increase the force applied to the chip base. A high excitation amplitude range is beneficial for mapping amplitude dependent resonance peaks of non-linear systems, and increases the adaptability during experimentation. For the acoustic horn, Titanium is chosen as material because of its excellent chemical resistance, and its characteristic impedance, which is in between PZT(Lead Zirconate Titanate) and Silicon[3]. Stainless steel is chosen as back mass material due to its high characteristic impedance, which relates to the mass the of the back mass scaled by its length at its first natural frequency[3].

3.2. Environment Chamber

As mentioned in chapter 2.3, spurious peaks could emerge in the response of the micro-cantilever in liquid due to the vibrational behavior of the environment chamber. Assuming the natural frequencies of the actuator lie outside the required bandwidth, the spurious peaks can either originate from the acoustic response of the liquid itself, or from resonances of the environment chamber structure, which travel through the fluid, to the cantilever.

An option would be to design the chamber in such a way that the first natural frequency is located above the required bandwidth. In practice such a design would be restricted to frequencies in the kHz range however, since the first natural frequency of the liquid itself, assuming a one dimensional case, is related to the dimension of the chamber by the following equation: $L = \frac{\lambda_{\text{liquid}}}{2} = \frac{c_{\text{liquid}}}{2f_0}$, where L denotes the characteristic dimension of the chamber, c_{liquid} denotes the speed of sound of the liquid, and f_0 denotes the first natural frequency. For instance, the dimensions of a chamber with a natural frequency of 1 MHz would be 750 µm, which is already fairly close to the typical length of an AFM cantilever (200 µm to 400 µm). The environment chamber designed around this liquid domain will probably have a natural frequency below the natural frequency of the liquid. An other limiting factor to the dimensions of environment chamber is determined by the squeeze film effect[4], of which the influence should be reduced to a negligible degree by selecting the chamber dimensions sufficiently large.

Opposed to making the chamber sufficiently small, the chamber could be fabricated of a high damping material to reduce the quality factor of the natural frequencies of the environment chamber[5] in addition to reducing the excitation on the liquid to a minimum by incorporating the chip of the AFM probe in the chamber wall. It is difficult to predict if the influence of the environment chamber is negligible though. A simulation, and preferably a modal analysis, of the full setup should be performed to ensure this.

[3] Appendix F.1
[4] Appendix C
[5] Appendix F.3

PTFE is chosen as the material[6] for the environment chamber and chamber base, because of its excellent chemical resistance, vacuum compatibility, and its characteristic impedance, which closely matches that of water. As a consequence, vibrations traveling in the liquid can transfer to the PTFE environment chamber where they are damped due to the relatively high material damping polymers generally possess. This increases the damping of the natural frequencies of the liquid in the chamber.

3.3. Integration

ITEM	PART NUMBER
1	Window Flange
2	DIN 912 M4 x 30 --- 30N
3	DIN 912 M4 x 8 --- 8N
4	O-Ring 14IDx1
5	Optical Window 20x1.1
6	Environment Chamber
7	AFM Probe
8	Chamber Base
9	Acoustic Horn
10	Piezo
11	Inertial Mass
12	Leaf Spring
13	Leaf Spring Mount
14	Thrust Washer 2.15x5
15	DIN 913 - M5 x 16-N
16	O-Ring 30IDx1.5
17	Lower Flange
18	Base Plate
19	3561 CK-M5-PK-3
20	FESTO Tubing 4 mm OD
21	Setup Holder

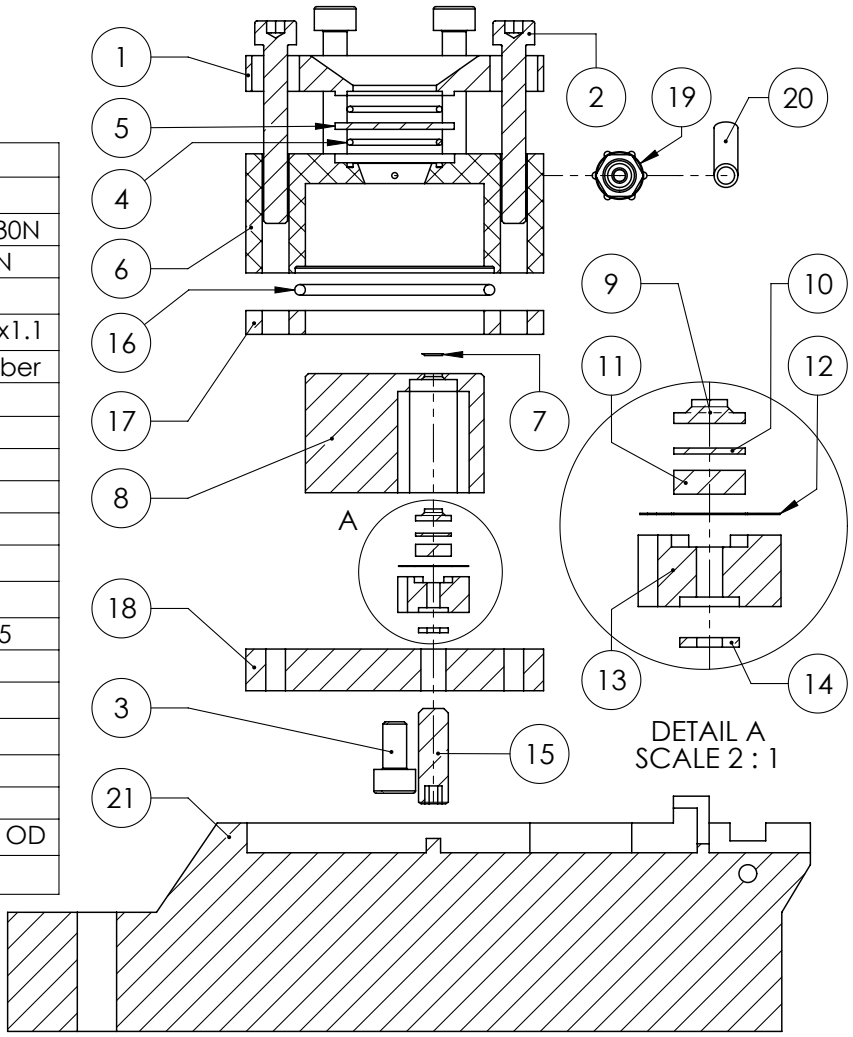

Figure 3.2: Exploded view of the setup as designed

Figure 3.2 shows an exploded view of the setup. Parts 1-6,8,9,16,17,19,20 make up the environment chamber, which can be divided into two parts. A base (parts 3,8,9,18) and a cap-shaped top (parts 1,2,4-6,16,17), which can be placed over the base.

The AFM chip (part 7) is clamped in between the environment chamber top (part 6) and the base (part 8), and is integrated in the chamber wall to minimize the amount of vibrations traveling from the actuator to the environment chamber. To mount the AFM chip, the chip should be placed on the acoustic horn, and the environment chamber, together with the lower ring and O-ring, is placed on top of the chip. Subsequently, the clamping force is applied by tightening the two bolts (part 2) which are in line with the AFM chip. These bolts go through holes in the lower flange and catch the tread in the base plate.

The environment chamber is sealed by tightening the remaining 4 bolts (part 2), which catch the tread

[6]Appendix F.1

in the lower flange, pulling the window flange (part 1) and lower flange together and compressing the O-ring seals (parts 4,16).

The actuator is integrated in a ring shaped part of the environment chamber wall, which is reduced in thickness and acts as a suspension for the actuator assembly. The piezo is electrically connected to the power source through a leaf spring (part 12), which is connected to the back mass, and through the acoustic horn, which is grounded. The leaf spring is of sufficiently low stiffness and ensures that no wires have to be attached to moving parts.

The cantilever vibrations can be inspected by laser Doppler vibrometer(LDV) through the optical window. Because the AFM Probe is incorporated in the chamber wall, the camera image of the LDV may slightly darken depending on the used objective lens and the medium in the environment chamber. However optical aberrations should not occur in theoretically because from the perspective of the optical system, the window flange, which is blocking the rays, is nothing more than a field stop[7]. The brightness of the image can easily be adjusted through the illumination settings of the camera.

3.4. Modeling of Actuator Behavior

To evaluate performance of the design, the vibration response of the actuator is modelled. After fabrication, the actual response of the chip base can be measured and compared to check the validity of the model. Apart from the response of the chip base itself, the response of the liquid at the chip base can be estimated, which is also exciting the cantilever. The response of the liquid is challenging to measure however, which increases the importance of an accurate model.

To increase insight into the physical behavior of the actuator, a one dimensional(1D) model comprising several components is studied, where the acoustic behavior of each component of the actuator is assumed to similar to that of a thin rod. Shear waves and the lateral inertia as a result of the Poisson effect are neglected in this analysis.

Hereafter a two dimensional(2D) finite element analysis is done to investigate the influence of shear waves and the Poisson's effect.

3.4.1. One Dimensional Analytical Model

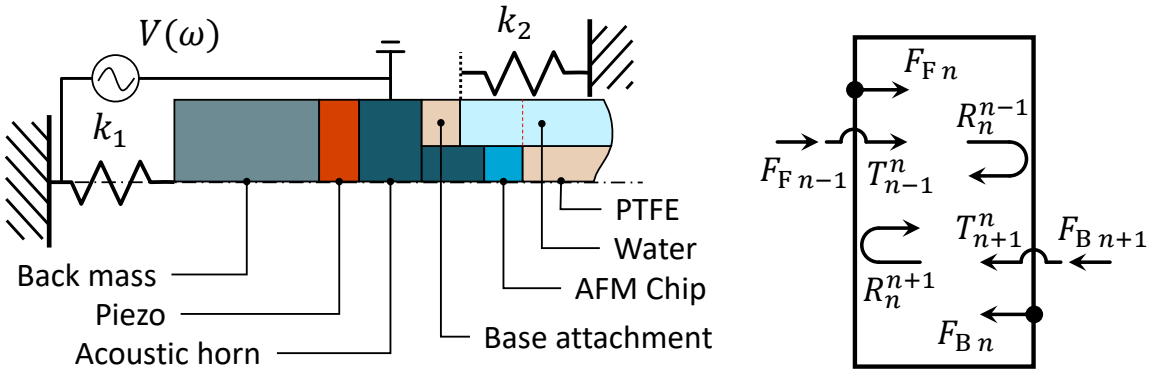

(a) Axisymmetric view of the one dimensional analytical model. The interface between the AFM chip and the PTFE is the point where the response of the chip base is calculated and the red dashed line denotes the place where the liquid response is calculated.

(b) Forward and backward traveling waves in a section

Figure 3.3: Schematic view of the analytical model

Figure 3.3 shows a schematic representation of the actuator modeled in 1D. The piezo is electrically connected through the leaf spring, which has a stiffness of k_1, and through the acoustic horn. The static stiffness of the actuator suspension has been calculated by finite element analysis, denoted by k_2. The response of each segment is governed by the wave equation (eq. 3.1):

[7] Appendix F.4

$$\frac{\partial^2 u}{\partial x^2} = \frac{1}{c^2_{\text{material}}} \frac{\partial^2 u}{\partial t^2} \tag{3.1}$$

where u denotes the particle displacement, x denotes the spacial dimension along the length of the actuator, t denotes the time, and $c_{\text{material}} = \sqrt{\frac{E_{\text{material}}}{\rho_{\text{material}}}}$ denotes the speed of sound in the material, dependent on its Young's modulus E_{material} and density ρ_{material}.

At the boundary of each segment the forces, and particle velocities, of the two adjacent segments should be equal. As a consequence, an incident wave coming from one domain will be partially reflected back, and transmitted to the next domain, depending on the boundary conditions. The transmitted and reflected waves can be calculated by multiplying the incident wave with the transmission and reflection coefficients respectively[54]. These coefficients can be calculated by solving each boundary condition for the situation where an incident wave is coming from infinite half-space, and the reflected and transmitted waves are traveling to infinite half-space, which leads to a boundary value system. These equations can be solved by realizing that:

$$\sigma = E_{\text{material}} \frac{\partial u}{\partial x} \tag{3.2}$$

where σ denotes the stress in the material. As a result $\dot{u}_{\text{transmitted}} = \frac{c_{\text{material}}}{E_{\text{material}}}\sigma$ and $\dot{u}_{\text{reflected}} = \frac{c_{\text{material}}}{E_{\text{material}}}\sigma$, assuming harmonic waves.

Combining these ratio's with the constitutive piezoelectric equations in Stress-Voltage form (eq. 3.3), the forces of the forward and back traveling waves can be calculated[55].

$$\mathscr{E} = -h\varepsilon + \frac{D}{\xi^{\varepsilon}} \tag{3.3a}$$

$$\sigma = E^D \varepsilon - hD \tag{3.3b}$$

where $\mathscr{E}$, h, ε, D, ξ^{ε}, σ, and E^D denote the electric field, the piezoelectric stiffness constant, the mechanical strain, the electric displacement, permittivity at constant strain, the mechanical stress, and the Young's modulus at constant electric displacement respectively.

A number of equivalent electrical circuit models[8] could be employed[55], which also integrate the electronic circuit. However, for sake of simplicity the electronic circuit is neglected. The response of the actuator is calculated by solving the system of boundary conditions, where $\sum F_{\text{forward}} = 0$ and $\sum F_{\text{backward}} = 0$ at each boundary, leading to equation 3.4. The particle displacement of the cantilever base and the liquid at the cantilever base (denoted by the red dashed line in fig. 3.3) are calculated by equation 3.5a and 3.5b.

$$\vec{b} = \mathbf{A} \frac{\vec{F}(\omega)}{V_{\text{act}}(\omega)} \tag{3.4}$$

where $\vec{b}$, $\mathbf{A}$, $\vec{F}(\omega)$, and $V_{\text{act}}(\omega)$, denote the vector containing piezoelectric material parameters and transmission ratio's, the matrix containing transmission and reflection ratio's, the piezoelectric material parameters and time delays for wave traveling from one boundary to the next, the vector of the forward- and backward traveling forces on the boundary, the actuation voltage respectively.

$$\frac{x_{\text{Chip}}}{V_{\text{act}}} = \frac{F_{\text{F Chip}} \exp(-\jmath\omega\tau_{\text{Chip}}) - F_{\text{B Chip}}}{\jmath\omega Z_{\text{Chip}}} \tag{3.5a}$$

$$\frac{x_{\text{Water}}}{V_{\text{act}}} = \frac{F_{\text{F Base}} \exp(-\jmath\omega\tau_{\text{Base}}) T^{\text{Water}}_{\text{Base}} \exp(-\jmath\omega\tau_{\text{Water@Chip}})}{\jmath\omega Z_{\text{Water}}} \tag{3.5b}$$

where x_{Domain}, V_{act}, $F_{\text{F Domain}}$, $F_{\text{B Domain}}$, τ_{Domain}, and Z_{Domain} denote the particle displacement, the actuation voltage, the forward traveling force, the backward traveling force, the amount of time it takes to travel across the length of the domain at the speed of sound, and the acoustic impedance respectively.

3.4.2. Two Dimensional Finite Element Analysis

To incorporate the effects of shear waves and the Poisson effect, a 2D axisymmetric Acoustic-Piezoelectric frequency domain finite element analysis is done, using the multi-physics interface of COMSOL. The setup

[8] Appendix D

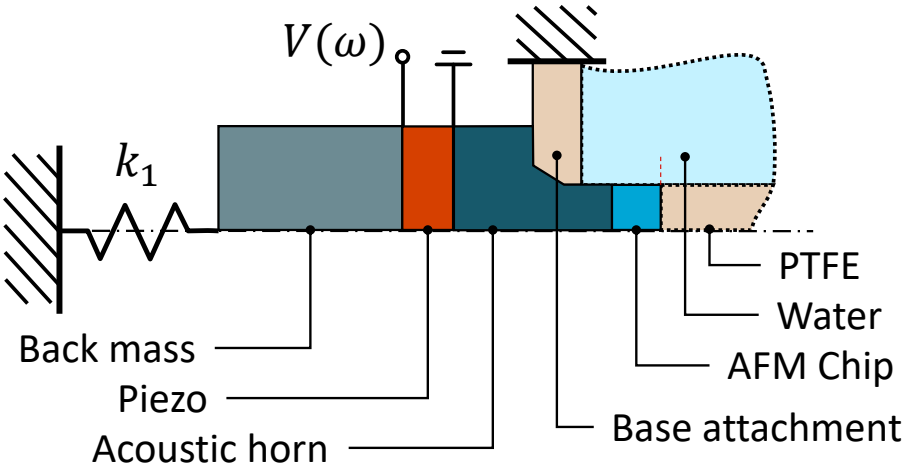

Figure 3.4: Axisymmetric view of the 2 dimensional finite element model. The interface between the AFM chip and the PTFE is the point where the response of the chip base is calculated and the red dashed line denotes the place where the liquid response is calculated. The acoustic and solid mechanic domains are denoted by dotted lines and solid lines respectively.

of the model is shown in figure 3.4 and can be divided into the pressure acoustics domain, the solid mechanics domain, and the electrostatics domain. The pressure acoustics domain is denoted by the dotted edges. In this domain only compressional waves are present. A perfect acoustic match is set on the outer edges of the acoustic domain to ensure there are no resonant frequencies associated with these domains, assuming vibrations entering the liquid and the PTFE environment chamber are completely damped out. The acoustic domain is coupled with the solid mechanics domain, which is denoted by solid lines, at the interfacing edges. The solid mechanics domain considers, in addition to compressional waves, also shear waves and the Poisson's effect. The solid mechanics domain is coupled to the electrostatic domain by the piezoelectric material of the piezoelectric element. A voltage of 8 V is applied to the piezo in the electrostatic domain. This voltage will also be used when the performance of the fabricated actuator is evaluated. The leaf spring is modeled as a spring k_1, distributed along the back end of the back mass. Opposed to the analytical model the suspension of actuator is not simplified as a spring, thus taking the higher-order resonances of the suspension into account. The suspension is fixed to the chamber base assuming the chamber base to be infinitely stiff. The response of the actuator is calculated at the cantilever base by taking the average absolute particle displacement parallel to the axis of symmetry at the front of the AFM chip. The response of the liquid is calculated by taking average of the absolute particle displacement parallel to the axis of symmetry at the red dashed line next to the location of the cantilever base. Since the acoustics domain only supplies the particle velocity the displacement is calculated by $u = \frac{v}{j2\pi f}$, where u denotes the particle displacement, v denotes the particle velocity, and f denotes the frequency.

3.4.3. Comparison of Models

Figure 3.5 shows the modeled response of the actuator. When comparing the analytical model to the FEA model, some notable differences can be observed. With the introduction of shear stiffness, the assembly can take up shear- and flexural deformations, next to the longitudinal deformations, which introduces modes below the first resonance frequency of the analytical model. This reduces the bandwidth from around 600 kHz to 370 kHz It is also observed that the liquid response form the FEA differs from the analytical model. This is due to higher-order modes of the suspension exciting the liquid. The lowest operation frequency is determined by the resonance/anti-resonance pair of the suspension mode of the actuator at 11 kHz.

3.5. Fabrication

Figure 3.6 shows the assembly process. Figure 3.6a shows the completed components of the setup. Most of these components are manufactured using a conventional lathe and mill (parts 1,6,8,9,11,13,17,18 from fig. 3.2), the leaf spring is laser cut and the setup holder is 3D printed. All other components are vendor parts. PTFE shows to be a difficult material to work because of its poor thermal conduction and high creep rate. Therefore it is advised to ease the requirements for chemical resistance and use a different material if a next

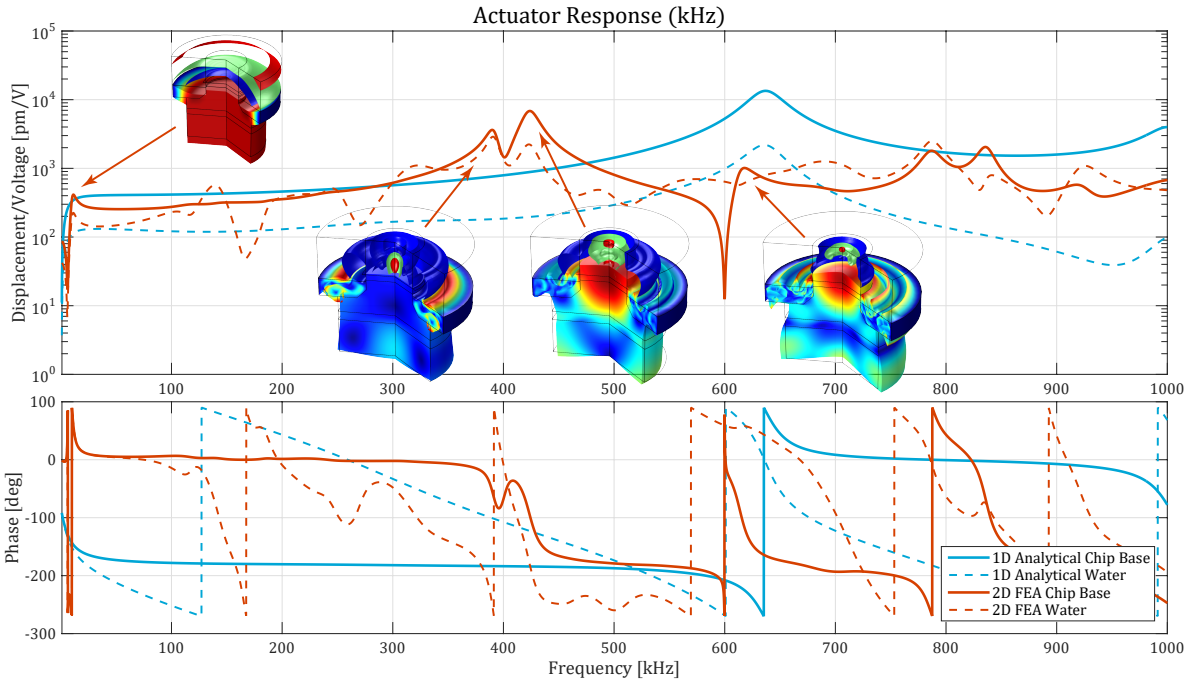

Figure 3.5: Modeled response of the AFM chip base, and liquid next to the chip, for the 1D model, shown in blue, and the 2D model, shown in orange. The suspension mode and the first three modes of the actuator are depicted close to their respective resonance peaks.

iteration would be made. Figures 3.6b and 3.6c show the assembly of the actuator. The electrical connection at the acoustic horn is made by carefully dispensing a droplet of conductive paint against the acoustic horn, while preventing the droplet from touching the back face of piezo, which would short circuit the piezo. The wire is dipped in the droplet of conductive paint and fixed with super glue. This connection is rather fragile however, so the setup should be handled with care. The piezo, back mass, leaf spring, leaf spring mount and live wire are assembled with conductive epoxy. It is important to note that the influence of the glue on the actuator performance is not a trivial issue, in this case however the influence is negligible given the thickness of the glue layer and its characteristic impedance[9]. Figure 3.6d shows the finished setup.

[9]Appendix F.5

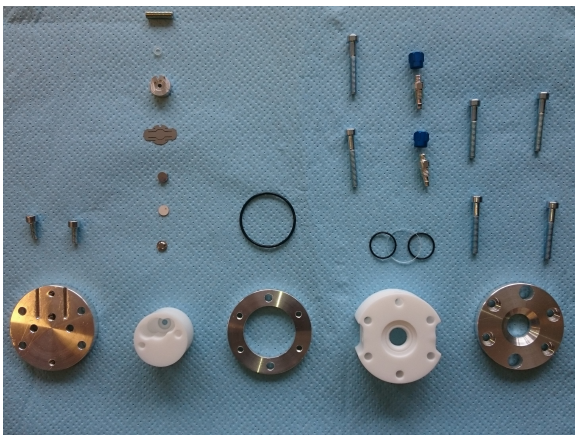

(a) Fabricated components and vendor parts, displayed from left to right the components from the bottom to the top

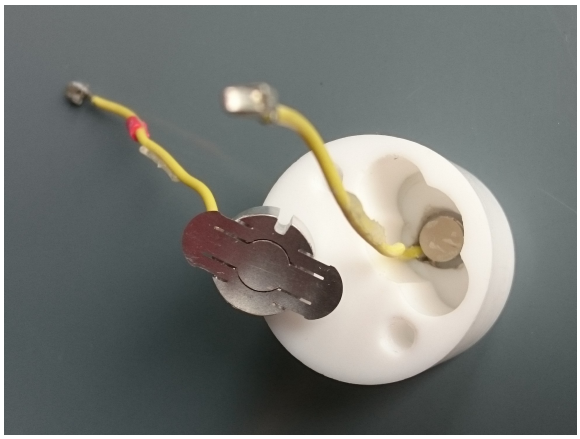

(b) Assembly of the actuator. The acoustic horn and the piezo are glued in the chamber base and the leaf spring is glued to the its mount.

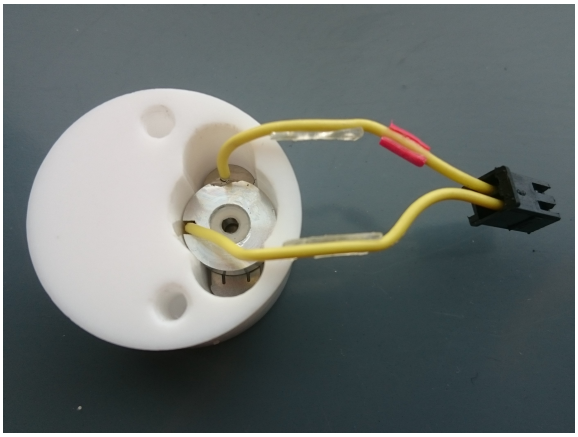

(c) Second step in the actuator assembly. The leaf spring and its mount is glued to the piezo

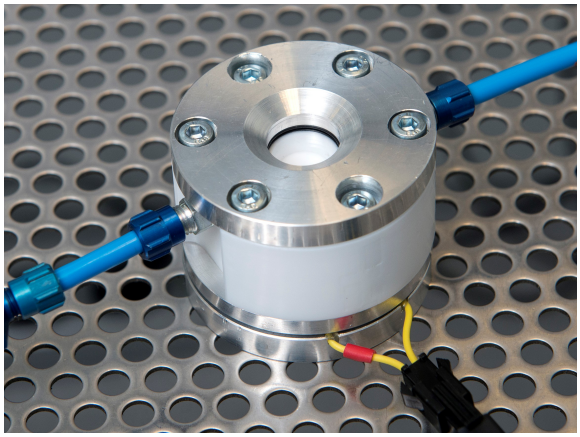

(d) The final setup as assembled

Figure 3.6: Setup fabrication

4

Design Validation

To validate the design and to investigate the response of micro-cantilevers immersed in liquid, the base motion of the actuator has been measured and the response of three different AFM cantilevers has been measured in air, vacuum and water.

4.1. Setup of Experiments

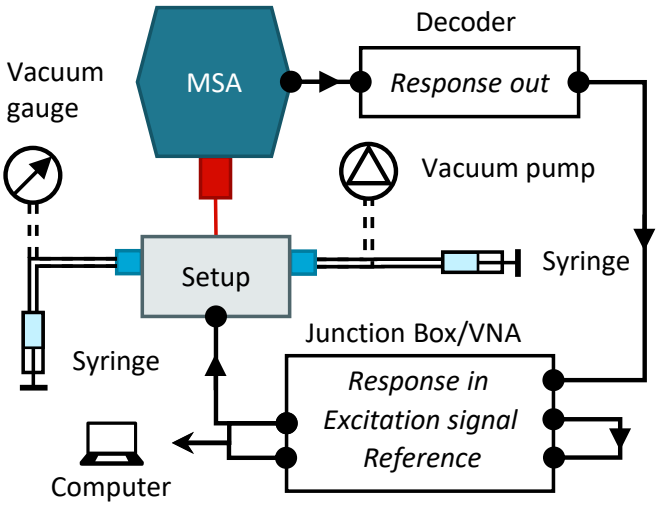

Figure 4.1: Schematic of experimental setup and auxiliary components. The arrows denote the direction of the data, the connection of the vacuum components are denoted by dashed tubes, and the connection of the syringes for liquid exchange are denoted by solid tubes.

Figure 4.1 shows the setup and its auxiliary components. The micro-cantilever is mounted in the setup and its vibrations are measured with a Micro-System Analyzer (MSA) LDV from Polytec Inc., of which the signal is fed into the decoder. The decoder translates the signal measured at the photo-detector of the MSA, which contains displacement and velocity data, into a electrical signal. This signal is fed into the junction box or the Vector Network Analyzer (VNA). Both also host the signal generator that provides the excitation voltage for the actuator. The measured response from the LDV and the reference signal (i.e. the excitation signal) is fed into computer for analysis. In contrast to the junction box, which does a fast Fourier transform (FFT) of the signal, the VNA uses a homodyne detection scheme, meaning it will only detect the response at the frequency of excitation.

The medium in the environment chamber can be exchanged by the in- and outlet ports on the setup (Festo 4 mm tubing connector). For the vacuum measurements a Pfeiffer vacuum gauge was attached to one end of the environment chamber and a Pfeiffer diaphragm pump, with an ultimate pressure of 0.5 mbar, to the other. For the measurements in water a syringe was connected to either side of the environment chamber.

One of the syringes is used to impose a negative pressure, while the other is used to expel liquid into the environment chamber. This procedure reduces bubble forming.

4.2. Actuator Response

The response of the acoustic horn and the chip base is measured and compared to the models of chapter 3.4. The actuator was excited by a pseudo random excitation signal. As shown in figure 4.2, the response of the chip base shows some decline in amplitude from 150 kHz and onward. This might be caused by the interface between the AFM chip and the acoustic horn, because the AFM chip is grooved. The models both assume a perfect circular interface, therefore the response of the acoustic horn gives a better representation of the actuator behavior. When comparing the measured response of the acoustic horn with the models, it can be observed that the 1D analytical model does not accurately describe the actual actuator response. The 2D FEA model however, gives a fair representation of the actuator response up to around 600 kHz. The first resonance frequency of the actuator is located at 377 kHz, which determines the bandwidth of the setup. This bandwidth can be extended up to around 550 kHz if the vibration response from the micro-cantilevers are scaled by the response of the base, i.e. examining the transmissibility. The operational deflection shape at the third resonance frequency (617 kHz) however curves the surface of the acoustic horn, introducing rotational effects on the base which cannot be compensated with the base response. Noise and small spurious peaks and drops are predominant in the region near the suspension mode of the FEA model and up to approximately 20 kHz. The excitation amplitude of the chip base has high variations in this region. This should be taken in consideration during the analysis of the cantilever response, because the energy fed into the system at those frequencies is irregular.

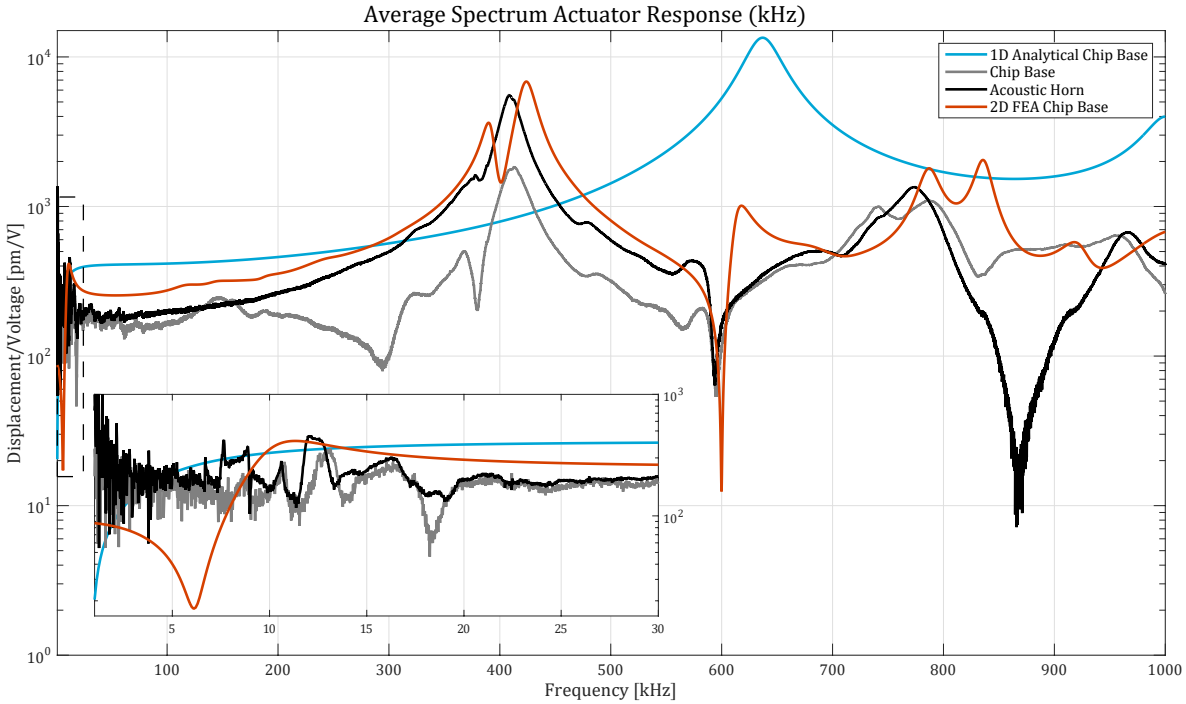

Figure 4.2: Measured frequency response of the actuator at the chip base and the top of the acoustic horn compared to the models. In the bottom left corner a zoom-in of the actuator response at low frequencies is shown.

4.3. Cantilever Response in Vacuum, Air and Water

The response of three different micro-cantilevers is measured in vacuum, air and water by exciting the cantilever with a frequency sweep. A vacuum of 0.6 mbar to 1.3 mbar was attained, which is fairly close to the ultimate pressure of the vacuum pump used. The three cantilevers are meant for different AFM operating modes and vary in dimensions and stiffness. The CONT cantilever is meant for contact mode AFM, where the tip of the cantilever drags across the sample mapping its topology. The stiffness of these cantilevers is usually relatively low to keep the applied lateral forces low, i.e. to reduce sample damage [56]. A variation on

this operation mode is force modulation mode AFM, for which the FMR cantilever is designed. In addition to the contact mode, the cantilever is vibrated to extract elastic properties from the sample. The NCLR cantilever is meant for tapping mode AFM, where the cantilever is excited at its first resonance frequency and strikes the surface of the sample, hence reducing lateral scanning forces and reducing damage of the sample as compared to contact-mode AFM.

4.3.1. Tapping Mode AFM Probe (NCLR)

The NCLR Tapping Mode AFM Probe, with typical dimensions 225(5) µm, 38(5) µm, 7.0(5) µm (length, width, thickness) has the highest first natural frequency of the three, 190 kHz. Figure 4.3 shows the transmissibility of the cantilever in vacuum at 0.6 mbar, air, and water. The measured first resonance frequency of the cantilever in vacuum is 152.47 kHz. Such a high variation in frequency is not uncommon though, which can be attributed to the fabrication process where tolerances of ±5µm in length and width, and ±0.5µm in thickness are typical.

Table 4.1 and 4.2 show the measured resonance frequency and the quality factor, identified by peak picking, next to the resonance frequency calculated with the Pade approximation derived by Sader and Van Eysden [1] and the quality factor derived by using Sader Method [2]. As expected the resonance frequency in air is hardly affected by the presence of the medium. Its quality factor however, drops from about 8000 to 500. Such a large drop is also observed in liquid, where the quality factor is about $\frac{1}{1000}$ of the value measured in vacuum and about $\frac{1}{100}$ of the value measured in air. The resonance frequency in water is about half the resonance frequency in vacuum and air. These values show good agreement with the estimated theoretical values taking into account that the aspect ratio can vary with 15 % according to the supplier. The resonance frequency measured in vacuum is used to calculate the fluidic resonance frequency, therefore, assuming the uncertainty in fluid density negligible, the aspect ratio is the parameter the greatest uncertainty. This uncertainty is reduced by varying the modeled cantilever dimensions within the factory tolerances until the resonance frequency in vacuum matches the measured resonance frequency in vacuum.

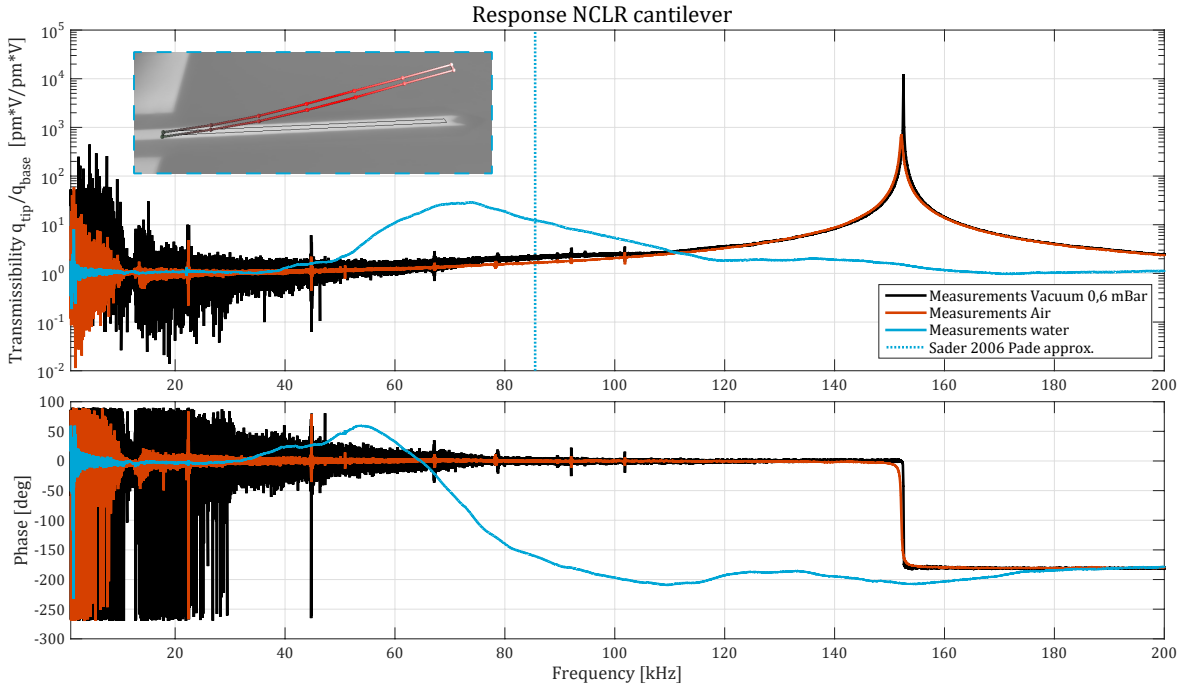

Figure 4.3: Measured frequency response of the NCLR cantilever with accompanying operational deflection shape of the first resonance frequency in liquid. The expected resonance frequency in liquid is denoted by a blue dotted vertical line, calculated with Sader's Pade approximation [1], using the typical dimensions as given by the supplier.

4.3.2. Force Modulation AFM Probe (FMR)

The FMR Force Modulation AFM Probe, with typical dimensions 225(5) µm, 28(5) µm, 3.0(5) µm (length, width, thickness), has a natural frequency of 75 kHz, in between those of the other two cantilevers. Figure 4.4 shows

Table 4.1: Comparison between the experimentally measured and theoretical [1] fundamental frequency of the NCLR cantilever in different environments

Mode	$f^{0.6\,\mathrm{mbar}}_{\mathrm{measured}}$ [kHz]	$f^{\mathrm{vacuum}}_{\mathrm{analytical}}$ [kHz]	$f^{\mathrm{air}}_{\mathrm{measured}}$ [kHz]	$f^{\mathrm{air}}_{\mathrm{Sader06}}$ [kHz]	$f^{\mathrm{water}}_{\mathrm{measured}}$ [kHz]	$f^{\mathrm{water}}_{\mathrm{Sader06}}$ [kHz]
1st flexural	152.47	152.76	152.07	152.27	72.10	85.51

Table 4.2: Comparison between the experimentally measured and theoretical [2] quality factor of the NCLR cantilever in different environments

Mode	$Q^{0.6\,\mathrm{mbar}}_{\mathrm{measured}}$ [-]	$Q^{\mathrm{air}}_{\mathrm{measured}}$ [-]	$Q^{\mathrm{air}}_{\mathrm{Sader98}}$ [-]	$Q^{\mathrm{water}}_{\mathrm{measured}}$ [-]	$Q^{\mathrm{water}}_{\mathrm{Sader98}}$ [-]
1st flexural	8214	497	680	7	9

the transmissibility around the first resonance frequency of the cantilever in vacuum at 0.6 mbar, air and water. Its first resonance frequency in vacuum (70.27 kHz) is located fairly close the natural frequency provided by the supplier. The second harmonic[1] of the first resonance frequency is also observed, close to 140 kHz. As with the NCLR cantilever, the resonance frequency drops significantly in water, however the resonance peak is rather irregular as opposed to the previous case.

Figure 4.5 shows the response of the cantilever, in the full bandwidth of the setup, in air and water. It can be observed that the second resonance peak in water does have a clear resonance peak. The measured and theoretical resonant frequencies and quality factors can be found in table 4.3 4.4.

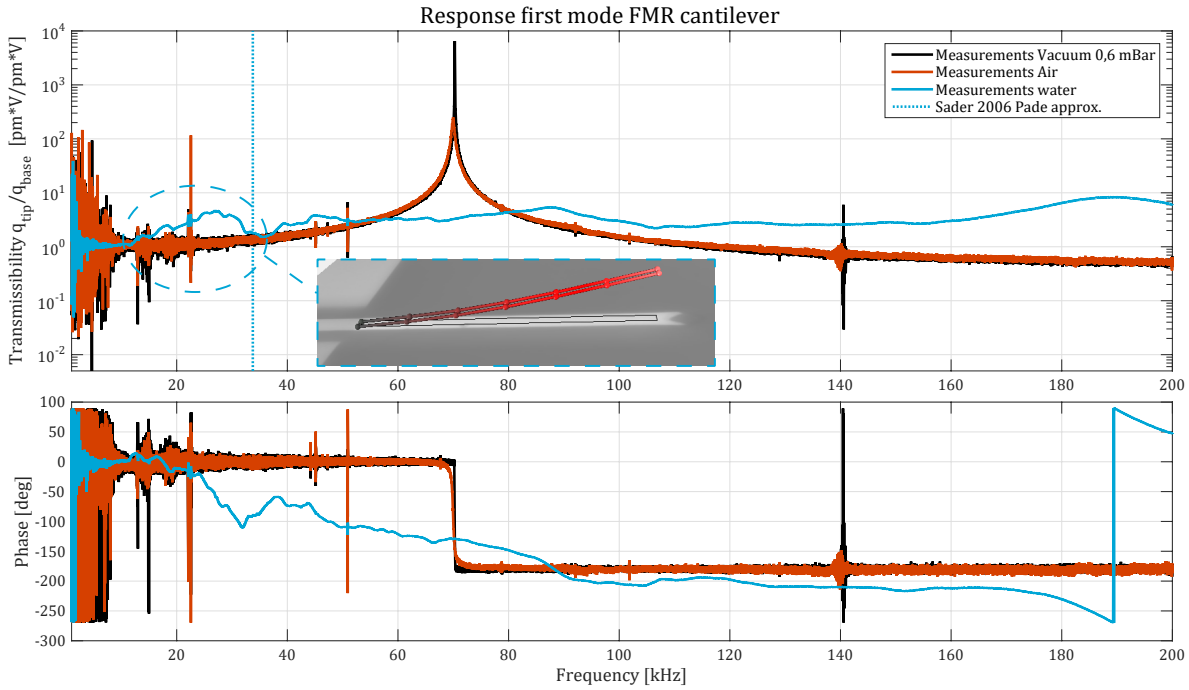

Figure 4.4: Measured frequency response of the FMR cantilever at the first mode with accompanying operational deflection shape of the first resonance frequency in liquid. The expected resonance frequency in liquid is denoted by a blue dotted vertical line, calculated with Sader's Pade approximation [1], using the typical dimensions as given by the supplier. The blue dashed ellipse surrounds the first resonance frequency in liquid.

[1] Appendix B

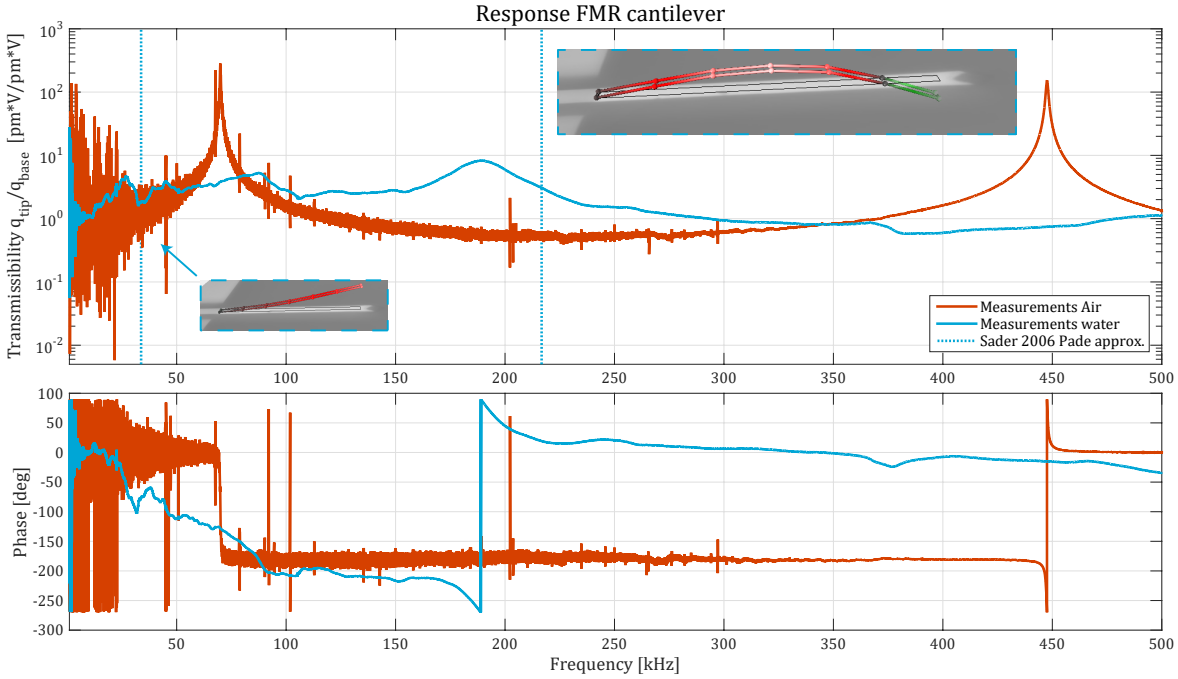

Figure 4.5: Measured frequency response of the FMR cantilever with accompanying operational deflection shape of the second resonance frequency in liquid. The expected resonance frequencies in liquid are denoted by a blue dotted vertical line, calculated with Sader's Pade approximation [1], using the typical dimensions as given by the supplier.

Table 4.3: Comparison between the experimentally measured and theoretical [1] resonant frequencies of the FMR cantilever in different environments

Mode	$f^{0.6\,\text{mbar}}_{\text{measured}}$ [kHz]	$f^{\text{vacuum}}_{\text{analytical}}$ [kHz]	$f^{\text{air}}_{\text{measured}}$ [kHz]	$f^{\text{air}}_{\text{Sader06}}$ [kHz]	$f^{\text{water}}_{\text{measured}}$ [kHz]	$f^{\text{water}}_{\text{Sader06}}$ [kHz]
1st flexural	70.27	70.85	69.93	70.13	26 ± 3	33.76
2nd flexural	-	444.03	447.10	443.18	188.65	216.71

Table 4.4: Comparison between the experimentally measured and theoretical [2] quality factors of the FMR cantilever in different environments

Mode	$Q^{0.6\,\text{mbar}}_{\text{measured}}$ [-]	$Q^{\text{air}}_{\text{measured}}$ [-]	$Q^{\text{air}}_{\text{Sader98}}$ [-]	$Q^{\text{water}}_{\text{measured}}$ [-]	$Q^{\text{water}}_{\text{Sader98}}$ [-]
1st flexural	5450	173	183	3	4
2nd flexural	-	451	503	7	8

4.3.3. Contact Mode AFM Probe (CONT)

The CONT Contact Mode AFM Probe, with typical dimensions 450(5) µm, 50(5) µm, 2.0(5) µm (length, width, thickness), has the lowest natural frequency of the three cantilevers, 13 kHz. This cantilever also has a significantly higher surface area compared to the other two. Figure 4.6 shows the transmissibility of the cantilever in vacuum 1.3 mbar, air, and water. As observed with the first resonance peak of the FMR cantilever, the second resonance peak of the CONT cantilever in water is irregular. The first resonance peak in liquid is not even observable. In an attempt to improve the quality of the response in liquid at low frequencies, the cantilever response was excited with a frequency sweep from 0.01 kHz to 50 kHz and measured with a more sensitive decoder, denoted by the dark blue line in figure 4.6. The quality of the response did not improve however. Also the resonance peak of first torsional ODS in liquid was not observed. Tables 4.5 and 4.6 show the measured, and theoretical, resonance frequencies and quality factors. The torsional resonance is calculated with the Pade approximation derived by Sader and Van Eysden [1] and the quality factor of the torsional resonance is derived by using Green and Sader [3].

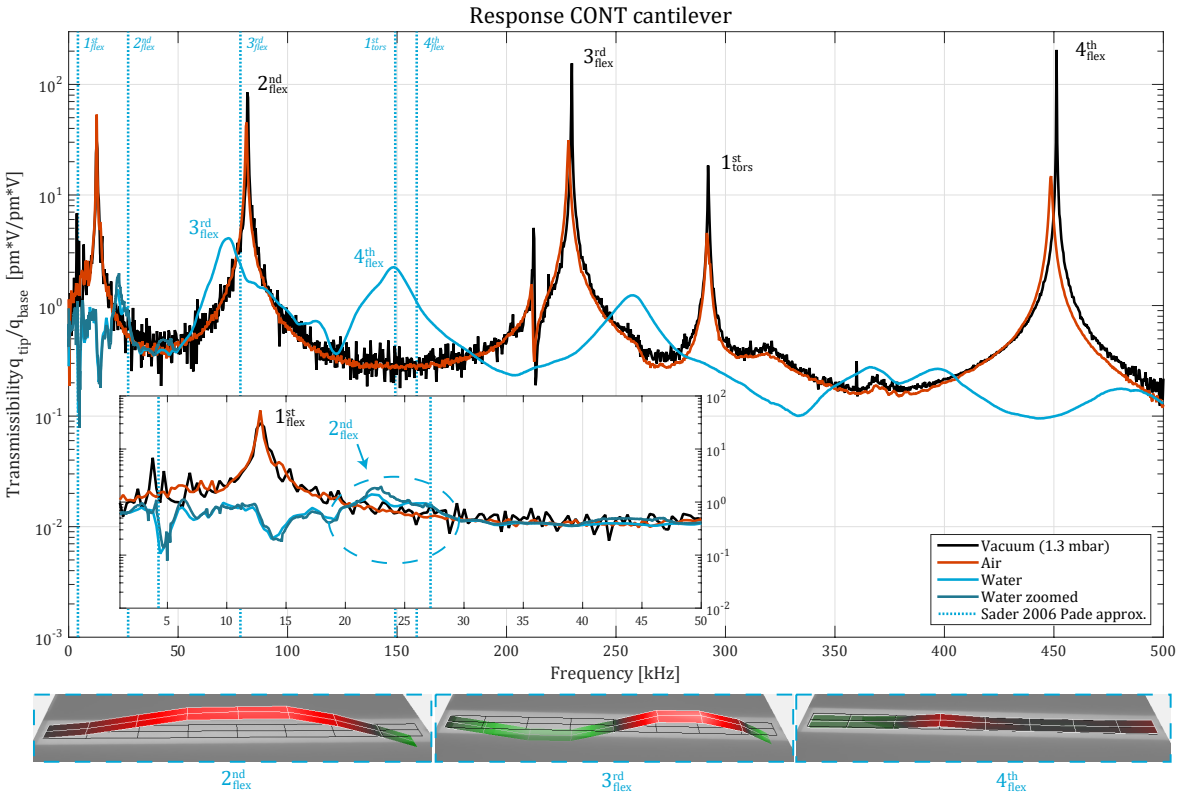

Figure 4.6: Frequency response of the CONT cantilever measured with the vector network analyzer (VNA). The expected resonance frequencies in liquid are denoted by a blue dotted vertical line, calculated with Sader's Pade approximation [1], using the typical dimensions as given by the supplier. The graph in the bottom left corner shows the response of the cantilever at low frequencies. The blue dashed ellipse surrounds the second resonance frequency in liquid. The operational deflection shapes of the second, third, and fourth flexural mode is depicted at the bottom the figure.

Table 4.5: Comparison between the experimentally measured and theoretical [1] resonant frequencies of the CONT cantilever in different environments. The torsional mode is emphasized.

Mode	$f^{1.3\,mbar}_{measured}$ [kHz]	$f^{vacuum}_{analytical}$ [kHz]	$f^{air}_{measured}$ [kHz]	$f^{air}_{Sader06}$ [kHz]	$f^{water}_{measured}$ [kHz]	$f^{water}_{Sader06}$ [kHz]
1st flexural	12.98	13.01	12.80	12.92	-	4.25
2nd flexural	81.80	81.55	81.22	81.41	25 ± 3	27.18
3rd flexural	229.88	228.34	228.44	228.83	71.58	78.46
1st torsional	*292.26*	*293.77*	*292.06*	*291.76*	-	*149.18*
4th flexural	451.40	447.46	448.89	449.49	148.71	158.98

Table 4.6: Comparison between the experimentally measured and the theoretical flexural [2], and torsional [3], quality factors of the CONT cantilever in different environments. The torsional mode is emphasized.

Mode	$Q^{1.3\,mbar}_{measured}$ [-]	$Q^{air}_{measured}$ [-]	$Q^{air}_{Sader98}$ [-]	$Q^{water}_{measured}$ [-]	$Q^{water}_{Sader98}$ [-]
1st flexural	277	59	54	-	2
2nd flexural	1638	168	154	3	5
3rd flexural	4437	291	261	7	8
1st torsional	4519	558	1037	-	7
4th flexural	5131	411	363	11	10

4.3.4. General Discussion of the Cantilever Response

The measured response of the micro-cantilevers in liquid, identified by peak picking, roughly matches the theoretical values derived by Sader, Green, and Van Eysden [1–3], as observed from table 4.3 to 4.6. The peaks

however are not Lorenzian, i.e. symmetric around the resonance frequency. This is observed with all three of the cantilevers. This increases the uncertainty of the curve fit used to estimate the quality factors and natural frequencies.

The observed irregular peaks and the missing first resonance peak of the CONT cantilever in liquid have some commonalities. They all: arose while measuring in water, arose below approximately 50 kHz, and have a theoretical quality factor below 5.

Above 50 kHz, no notable spurious peaks where found in water, although some small local increases in amplitude can be observed. The amplitude of these peaks is much smaller however compared to the amplitude of the cantilever resonance peaks in water.

5

Conclusion and Recommendations

The conclusion is divided up into two sections. The first discusses the performance of the setup, and the second the measurements done with the setup. Hereafter, the recommended improvements to the setup and the different directions for future work are elaborated upon.

5.1. Setup Performance

A setup was designed using design principles for ultrasonic transducers. Its performance is evaluated by comparing it with the initial requirements[1].

Bandwidth

The objective was to design a setup with a bandwidth of 1 kHz to 1000 kHz. As a result of fabrication limitations this was reduced to 10 kHz to 550 kHz. This range is large enough to excite up to 4 flexural cantilever modes in vacuum and air given the first natural frequency is chosen between 10 kHz to 15 kHz. The response of the setup between 10 kHz to 20 kHz is irregular though, showing small spurious peaks and drops in amplitude. These could complicate measurements at this frequency range, especially in liquid due to the low quality factor of the modes.

Measurement Quality

Eliminating spurious peaks, especially in liquid was one of the main challenges of this project. The response of the actuator shows some small spurious peaks at 10 kHz to 20 kHz and the response of the FMR, and CONT, cantilevers was irregular below 50 kHz. A clean response is found from 20 kHz to 500 kHz in vacuum and air, and from 50 kHz to 500 kHz in water.

Setup Versatility

The setup was designed to be versatile with respect to sample selection, and operating environment. The setup allows modal testing of cantilevers coated with a special materials (piezoelectric, magnetostrictive, magnetic, etc.), as well as bare silicon cantilevers. The clamping mechanism also facilitates easy exchange of the AFM chip.

The environment chamber was build such that it can be used for measurements in: vacuum, different types of gasses, and different types of liquids including mild acids and alkalies, common alcohols and oils. The desired vacuum level was set at 10^{-3} mbar to ensure, however due to available equipment this level of 1.3 mbar to 0.6 mbar was obtained. The flow regime at this pressure can be estimated by evaluating the Knudsen number $Kn = \frac{\lambda}{L}$, where λ and L denote the mean free path and characteristic length scale respectively. The cantilever width is the characteristic length scale in case of vibration cantilevers [2], which is 50 µm for the largest measured cantilever (CONT). The mean free path at 1 mbar is approximately 100 µm, which result in a Knudsen number of 2. This is somewhere in the transitional flow regime [57]. To reach the molecular flow regime, where viscous damping is negligible, a vacuum level below 10^{-1} mbar would be mandatory. This level should be achievable with a vacuum pump with a higher ultimate pressure. To reach the structural damping regime where free molecular flow damping is negligible, an even higher vacuum level is required. The setup

[1] Appendix A.1

was also designed to be modular, so the current environment chamber could be exchanged for a separate vacuum chamber designed for high vacuum for instance.

Modal Analysis

The ambition was to do a single-degree-of-freedom(SDOF) modal analysis of a micro-cantilever in vacuum, air, and water and compare the results to the results of a multi-degree-of-freedom(MDOF) modal analysis. The available modal analysis software SDTools however, was to complicated to master in the span of a graduation project next to the design and validation of the setup. A MDOF identification will probably improve the identification accuracy, especially in liquid where the modes are highly damped and closely spaced.

5.2. Dynamic Behavior of Micro-Cantilevers in Vacuum, Air, and Water

Resonance peaks could successfully be in measured liquid from 50 kHz to 500 kHz. It was observed however, that the shape of all peaks in liquid are not Lorenzian. This could be caused by highly damped spurious peaks located directly behind the resonance peaks, however seems unlikely since this behavior was observed at all the resonance peaks of all the cantilevers measured, which had resonance peaks located at different frequencies. One would expect to see the spurious peaks in the response of all cantilevers at the same frequency. This is not the case. An other explanation might be that due to the intensity of excitation, or the way the force is applied with base excitation, nonlinearities emerge.

It was also found that the first resonance peaks of the flexural and the torsional mode of the CONT cantilever was not observed in the cantilever response in water. From table 4.5 and 4.6 can be concluded that the resonance frequency of the first flexural mode is probably located outside the actuator bandwidth, where the amplitude of base excitation is rather low. In addition, the peak has quality factor of 2 according to Sader's model [2], which would make it extremely difficult to observe in the region with a irregular actuator response. The resonance frequency of the first torsional mode is located very close to that of the fourth flexural mode. Due to the high damping in liquid the torsional mode might overlap with the third or forth flexural mode. From the transmissibility (fig. 4.6) response of the CONT cantilever a small peak at approximately 120 kHz can be observed. It was not possible to relate the ODS at this frequency to the first torsional mode however, due to the large base excitation at this frequency compared to amplitude of the torsional resonance. The Polytec software is unable to calculate the transmissibility to use during ODS analysis. The ODS in addition will be a combination of the torsional mode and the third and/or fourth mode, which would require sophisticated MDOF identification techniques to confirm the exact location and quality factor of the torsional mode.

As discussed in chapter 4.3.4, the first mode of the FMR cantilever and the second mode of the CONT cantilever show irregular resonance peaks. This might be caused by the actuator, which has a low excitation amplitude and a irregular response at lower frequencies. As a result the modes might not be not fed enough energy to build up due to their low quality factor. An other reason could be that resonance peaks of the liquid are interfering with the resonance frequency of the modes. Although no resonances from the liquid have been observed at the frequency range in question in the response of the NCLR cantilever, which has no resonance frequencies in this range. The NCLR is less susceptible to influences of resonances from the liquid however, because of its dimensions and relatively high stiffness.

5.3. Resolving the Research Question

The research question driving this project was defined as: ***How can modal testing of micro-cantilevers immersed in liquid be performed properly[2] ?***

The answer is: analyze the dynamics of the entire setup, including the environment chamber and the liquid contained. To truly eliminate all the spurious peaks. In case of base excitation the setup can only be excited to its first resonance frequency(be it from the actuator, the liquid or the environment chamber). This limits base excitation to either low frequencies, so the first resonance frequency of the setup is not excited, or very high frequencies, where the first resonance frequency is suppressed by a highly damping material which matches the acoustic impedance of the liquid. Achieving a design in between these two extremes is difficult due to fabrication limitations. Other excitation methods, such as magnetic excitation, do not suffer from these limitations because they are not in direct contact with the environment chamber and, therefore do not excite the environment chamber. The influence on the dynamics of the system under test however, due to

[2] Low coupling between setup vibrations and sample, low signal to noise, low influence on the dynamics of the system under test

added mass and stiffness, is high compared to base excitation, which is undesirable during modal testing. These actuation methods are only advantageous if the system under test already has the required layer in its design, essentially making it a form of operational excitation as discussed in chapter 2.1. Lastly, Brownian excitation, which also does not excite the environment chamber, has a high noise level and no reference of the excitation force. As a consequence the dynamics of the system under test can only be examined by operational modal analysis techniques.

5.4. Recommendations

Improvements and future work could be done on the following topics:

Improvements to the Setup

The current setup could be improved by altering the design of the actuator slightly to ease the assembly of the electrical wire connection to the acoustic horn, as discussed in chapter 3.5, and by improving the tension relieve on both of electrical wires. This would make the design more robust. A lot of fabrication issues where also encountered due to the use of PTFE, which is difficult to work. As a result, the acoustic horn did not slightly stick out of the environment base, which would have allowed to measure the cantilever response from the top of the cantilever. Also the environment base was intended to act as a guidance for the cap-shaped top. Fabricating a tight fitting on these parts was not achieved. PEEK could be used as an alternative material. It has a lower chemical resistance than PTFE, but is more stable during fabrication. It also has a low outgassing.

Check Transmissibility with the Polytec

The Polytec software is currently only able to analyze the transfer functions obtained, however if these transfer functions could be divided by the average excitation at the base of the cantilever, the analysis of the operating deflection shapes and resonance peak will probably become more accurate and modes in liquid will be more easy to detect.

Feed Forward Control

Currently the actuator has a low excitation amplitude at its lower frequency range compared to the excitation amplitude close to its first resonance frequency. This might be circumvented by controlling the excitation voltage by feed forwarding the inverse dynamics of the actuator.

Design high-frequency and low-frequency setup

To increase the understanding of the fabrication limits encountered during the design, a separate high and low frequency setup can be build and their performance could be compared to the current setup. The low frequency setup could be designed with a environment chamber close to the dimensions of the cantilever and be excited as a whole. The bandwidth of this setup would be determined by the first resonance frequency of the liquid or environment chamber. Because the setup is excited as a whole, the cantilever doesn't have to be mounted inside the chamber wall and the setup would be easier to seal. Because the mounting wouldn't have to be integrated in the chamber wall, modal testing does not have to be restricted to micro-cantilevers. The high frequency setup would consist a piezo integrated into an environment chamber made from a highly damping material with a impedance close to the liquid. This design would not need an inertial back mass, because the environment chamber would act as the backing material.

Other forms of base excitation

In addition to piezoelectric base excitation, other forms of base excitation exist, such as magnetostrictive and electromagnetic for instance. These might be coated with a corrosion resistive material. Since these do not require electrical wires at the place of excitation, the risk of short circuit disappears. These techniques are already used in electromagnetic acoustic transducers (EMAT).

Force Detection

The current setup can not be used to determine the mass and stiffness of the micro-cantilevers unless a model is used to match the different resonance frequencies. If the force on the cantilever could be accurately detected, this could be done experimentally. This might be done by installing a sensing piezoelectric patch at the chip base, or by calculating the force on the cantilever with the measured excitation amplitude of the base, for example. Measuring the forcing remains a challenge for microsystems however.

Mounting
The effect of the mounting on the response of microsystems in general has had very little research. An experimental comparison of these methods would be of great value to research and develop in the AFM industry, but also for the MEMS packaging industry, who might want to suppress ambient vibrations.

Non-Lorenzian Shaped Peaks in Liquid
It was observed that the resonance peaks in liquid were non-Lorenzian. The case of this could be investigated by analyzing the response of the cantilever in liquid excited by Brownian forcing and comparing this response to the response found with base excitation at different excitation voltages, starting at very low voltages and by slowly increasing it.

Vacuum Chamber
The current vacuum chamber is limited to about 1 mbar. It might be interesting however, to monitor the quality factor while pumping down to higher vacuum levels. The transition from the viscous regime through the slip regime, transitional regime, and free molecular regime into the structural damping regime can be mapped out in this fashion. This has be done before in literature [53], however in the structural damping regime all damping from the gas in the chamber can be neglected, which makes this a perfect reference point for fluid identification. To achieve these high vacuum levels, a pump with a lower ultimate pressure is necessary, and possibly a modified environment chamber optimized for high vacuum.

Modal Analysis
A MDOF modal analysis method was not be used to identify the modal parameters in liquid. To increase the accuracy of the parameter estimation, a MDOF identification is highly advised because of the close spacing of the highly damped cantilever modes. It would also be interesting to compare the mode shapes in liquid to the mode shapes in air and vacuum. The fluid-structure interaction might slightly change the shape of the mode.

Operational modal analysis techniques may be used to in addition to experimental modal analysis to compensate for the lack of information about the forcing, since currently fluidic forcing acting on the cantilever in addition to the base excitation is not measured. Using operational modal analysis to identify modal by Brownian excitation might also give more insight into the behavior of micro-cantilevers in liquid. Literature has not gone further than identifying natural frequencies and quality factors by peak picking.

Modal testing of plates immersed in liquid
Next to cantilevers, plates are common elements in microsystems [58] and a setup of experimental modal analysis for plates might be a next step after modal analysis on cantilevers has been explored. Plates often have many closely spaced modes, even in air. This is because they have a similar bending stiffness in multiple directions. Because of their relatively large surface area they are more sensitive to added mass and damping, which could be exploited to do rheological measurements on gasses for example. They are also used to measure rheological properties of liquids [59]. A rigorous modal analysis would provide the researcher with information on changes in stiffness, mass, damping and mode shapes of multiple modes. This information could reveal properties of the adhered particle.

A

Project Confines

Below the confines of the project are set. This is done to ensure research stays on topic and no time will be spend on unnecessary features.

A.1. Requirements

General

Measurement quality: The response should be clean, without spurious peaks

Vibration type: Out of plane vibrations

Sample types: AFM cantilever (coated and uncoated)

Environment

Medium: Liquid water, air, and vacuum (all other units should be vacuum and liquid compatible)

Vacuum level: Air resistance negligible ($< 10^{-3}$ mbar)

Actuation

Bandwidth: 1 MHz

Excitation type: Single degree-of-freedom harmonic, and random

Excitation force: Non-linear excitation in vacuum and air, linear in liquid

Mounting

Force type: May not effect cantilever

Operation: Sample easily interchangeable

Modal Analysis

Domain: Frequency domain

Parameter estimation: Compare results of single-degree-of-freedom with multi-degree-of-freedom in air/vacuum and liquid

A.2. Scope

- The test platform will solely be developed to test AFM cantilevers
- The measurement system will be restricted to the laser Doppler vibrometer (LDV) available at the university, the Polytec MSA
- The electronics necessary for driving the actuator, such as the frequency generator etc., will not be designed by the student

A.3. Constraints

- The supervisors have to be available for consult
- The necessary facilities have to be available, e.g., computers, laboratory space and equipment, and software.
- There has to be a budget for the production of the prototype
- AFM cantilevers have to be available for testing

B

Modal Testing

Modal testing is a experimental method to characterize the dynamic behavior of a certain system from its vibrational response. The assumption is made that the system's dynamic behavior can be expressed by its mode shapes and its modal parameters: natural frequencies, modal masses, modal stiffnesses, and modal damping ratios. The shape of these modes are described by a summation of waves and defined by the way the system would naturally oscillate between the elastic- and kinetic energy, if a certain amount of energy where to be present in the system. The natural frequencies at which these oscillations would occur depend on the distribution of mass, stiffness and damping throughout the system. The modal mass, modal stiffness and modal damping ratio express the amount of mass, stiffness and damping that contributes to a certain mode, as if it where to be a single degree of freedom mass-spring-damper system.

Modal testing is a linear technique in its origin and the majority of this chapter assumes the system in question to behave in a linear or weakly nonlinear manner. With this assumption the system can be described mathematically by equation B.1 where: **M** denotes the mass matrix, **C** denotes the damping matrix, **K** denotes the stiffness matrix, $\vec{q}(t)$, and its derivatives, denote the motion of the structure, and $\vec{f}(t)$, denotes the force applied to the structure.

$$\mathbf{M}\ddot{\vec{q}}(t) + \mathbf{C}\dot{\vec{q}}(t) + \mathbf{K}\vec{q}(t) = \vec{f}(t) \tag{B.1}$$

Nonlinear behavior is certainly present in practice though, and a linear description of the system might be an oversimplification in certain situations. In such situations, nonlinear modal analysis could provide further insight, as discussed in (Kerschen, 2014) [60]. Though specifications of the sensor or the actuator might vary for example, the experimental set up for both cases are similar[61].

This chapter starts with a general introduction of modal testing, which is based on the works of (Ewins, 2000) [24] and (Brincker, 2015) [62]. The latter is focuses on operational modal analysis. These works are recommended for further reading. Modal testing can be divided in two phases. The data acquisition phase, and the modal analysis phase, where the acquired data is analyzed. A fundamental understanding of each phase is critical for the design of a modal test setup. The modal test procedure is shown in figure B.1. After the general introduction, the advancements in modal testing of microsystems is discussed.

B.1. Data Acquisition

During modal testing the system is excited by a harmonic force. The resultant vibrations are determined by measuring the displacement of the system, or one of its derivatives, at a certain location on the structure. In this way the frequency response is obtained, the measure of magnitude and phase of the output with respect to the input, as a function of frequency.

To determine the dynamic characteristics of the system, this frequency response measurement is repeated for multiple excitation- and measurement locations, resulting in a matrix of frequency response functions. This process is shown in step 1 and 2 of figure B.1. As an example, a plate is used as device under test. $F(\omega)$ denotes the harmonic input force to the system and the displacement q, or one of its derivatives, denotes the measured response at a certain location. The amount of locations measured and excited determines the amount of observable eigenfrequencies. Theoretically due to the symmetry of this matrix, explained by Maxwell-Betti reciprocal work theorem, the dynamical behavior of the system can be obtained if only the

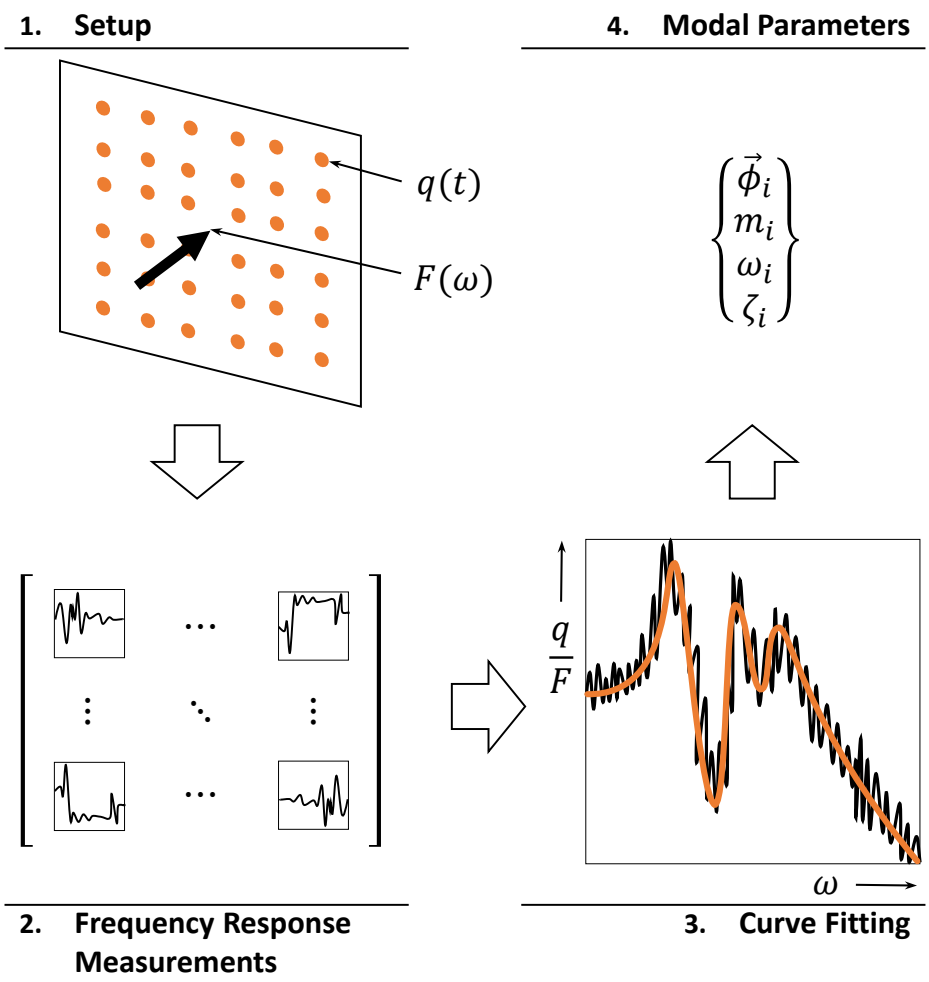

Figure B.1: Schematic of the modal testing procedure. $F(\omega)$ denotes the harmonic input force and the displacement $q(t)$, or one of its derivatives, denotes the measured response at a certain location. The modal parameters $\vec{\phi}_i$, m_i, ω_i, ζ_i, denote the mode shape, modal mass, modal frequency and modal damping of each mode i respectively

vibration at one location is measured while the system is excited at multiple locations, or only one location is excited while the vibrations at multiple locations are measured. This equivalates to obtaining either one of the rows, or one of the columns, of the frequency response matrix. The former approach is used during the impact hammer test and the latter is used during spectral tests using electrodynamic shakers. In practice however, the obtained information is not always adequate to determine the dynamic behavior of the system due to the complexity of the system, or the desired accuracy, and multiple rows or columns have to be obtained. The extensiveness to which modal tests are done can be divided into different levels as defined by Ewins [24].

Level 0: estimation of natural frequencies and damping factors; response levels measured at few locations; very short test times.

Level l: estimation of natural frequencies and damping factors; mode shapes defined qualitatively rather than quantitatively.

Level 2: measurements of all modal parameters suitable for tabulation and mode shape display, albeit not normalized.

Level 3: measurements of all modal parameters, including normalized mode shapes; full quality checks performed and model usable for model validation.

Level 4: measurements of all modal parameters and residual effects for out-of-range modes; full quality

checks performed and model usable for all response-based applications, including modification, coupling and response predictions.

B.1.1. Operating Deflection Shapes

When measuring the vibrational deflection of a system at enough locations, the operating deflection shapes of the system can be described. An operating deflection shape (ODS), is the systems vibrational deflection shape at a particular frequency under influence of a certain excitation. Changes in excitation will influence the ODS.

Each ODS can be described as a weighted superposition of the systems mode shapes, as shown in figure B.2. The mode shapes are inherent to the dynamics of the system and do not depend on the applied excitation, the weighting of these modes does however. At a certain resonance frequency the ODS can be considered equal to the mode shape of which the natural frequency relates to the concerned resonance frequency, if the system is lightly damped and the natural frequencies of the modes are well spaced. The influence of the other modes at that frequency are assumed negligible. During the modal analysis the frequency response functions (FRF) and operating deflection shapes are used to extract the dynamic characteristics of the system in the form of the modal parameters, and the mode shapes. These dynamics characteristics can be used to create a dynamical model of the system.

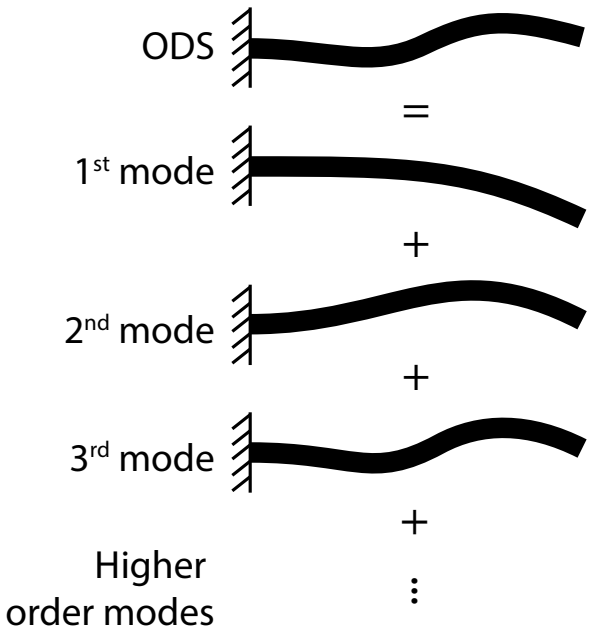

Figure B.2: Operational deflection

B.1.2. Harmonics

The vibration response is measured in the time domain. For frequency domain analysis the response is usually converted to frequency domain by a fast Fourier transform (FFT) algorithm. Apart from the previous discussed resonance peaks, additional peaks might appear in this frequency response. These peaks will appear at a integer multiple (or multiplicative inverse integer) of the resonance frequencies. These harmonics are caused by the nonlinearity of the system. Imagine the system being excited at a single frequency by a perfect sinusoidal force and being measured at a single point. This input- output behavior is described by the transfer function of the system, and if the system where to be linear, this would result in a perfectly sinusoidal output at the same frequency. However, if the system is nonlinear the output will not be a perfectly sinusoidal signal anymore. This periodic signal introduces harmonics in the FFT, which is a summation of perfect sinusoids to describe the periodic output signal.

B.2. Modal Analysis

Once the data acquisition is carried out the next step is to analyze the obtained data. Modal analysis can be divided into two types: experimental modal analysis (EMA) and operational modal analysis (OMA). Experimental modal analysis is the most well-known of the two. The data needed for these types of analysis define the data acquisition procedure and the required test setup.

During experimental modal analysis the system is excited by a known force. This is done either by measuring the force applied directly, or, if the dynamic behavior of the actuator is well-known, by deriving the force from the input signal of the excitation device.

In the case of operational modal analysis the excitation force is not known. The frequency response of the system is measured in "operation" while the structure is excited by ambient vibrations and other environmental effects (waves, wind, etc.). These excitation forces are assumed as white noise excitation. There are some conditions for these ambient excitation forces to allow modal analysis of structures with closely spaced natural frequencies though. In essence, the random distribution of forces should be such, that the excitation can be considered a multiple degree of freedom input. Also, the scaling of the weight of each mode in a certain ODS can be challenging. One solution is to perform a second frequency response measurement of the system with a known added mass or stiffness, which is not always practical. An other solution is to use the mass matrix of a finite element analysis (FEA) of the system during the modal analysis.

Civil engineering is one of the main application fields of operational modal analysis. Due to the size of these structures it is not always feasible or advantageous to properly excite these structures with a well-know or measured force. This situation shows much resemblance with microsystems, where the applied force of certain excitation methods is difficult to determine accurately.

The identification of the modal parameters of a system can be done in various ways. The simplest, known as "peak picking", is to fit the curve of each resonance peak to the theoretical frequency response of a single degree of freedom (SDOF) mass-spring-damper system. The mode shape in this case is assumed equal to the ODS at that resonance peak. However, this technique is not sufficient if a high accuracy is required , closely spaced modes are present, complex modes are present, or if the system shows nonlinear behavior. In those cases either more intensive, multiple degree of freedom (MDOF), techniques are required, or nonlinear techniques.

The existence of closely spaced modes depends on the geometry of the structure. For instance, a beam with approximately equal flexural stiffness in different directions of its cross section, a plate with approximately equal dimensions on different directions, or structures with nearly equal flexural and torsional stiffness. As a consequence the natural frequencies, and thus resonance peaks, in such systems are closely spaced. Especially in highly damped systems, the mode shapes belonging to the closely spaced natural frequencies influence both of the operating deflection shapes at the related resonance peaks.

Apart from complicated identification, closely spaced modes can also lead to complex modes. While normal modes can be described by standing waves, complex modes can only be described by traveling waves. Complex modes arise as a consequence of non-proportional damping distributed throughout the system [24], i.e., the damping **C** shown in equation B.1 is not proportional to the mass and/or stiffness[63], as would be the case with proportional damping[24].

B.3. Modal Testing of Microsystems

Microsystem dynamics differentiates itself from macro-scale dynamics due to the high coupling between the different energy domains and nonlinear behavior[4], e.g., the dynamic behavior of the coupled fluid-structure interaction inherent to structures submerged in liquid, as will be elaborated in chapter C, can only be assessed *in situ*. Measuring the dynamic response of the fluid and the structure separately and superimposing the results afterwards would not suffice. These effects would have to be assessed simultaneously.

Modal testing of microsystems is not a simple translation from the macro-scale to the micro-scale, due to their dimensions. For example, a microsystem cannot be properly excited by an impact hammer, and a conventional shaker is unable the excite the high frequency (typically kHz to MHz and possibly even GHz) responses present in microsystems [6]. Apart from the excitation itself, the measurement of this excitation force and the induced vibrations also pose a challenge. Lin *et al.* reviewed the current state of microsystem dynamics in 2006 [6]. Methods for measuring vibrations in microsystems have been well established [17, 21, 30, 31, 64–72], especially for out-of-plane vibrations, vibrometers for microsystems are commercially available. A variety of excitation methods have also been researched. The measurement of these excitation forces remains a challenge though. In the case of piezoelectric base excitation, a popular excitation method

for modal analysis of microsystems in vacuum or air[64, 65, 73, 74], the sensing layers in piezoelectric actuator allow for direct measurement of the excitation forces to the attached structure. However, in most cases the excitation force can only be derived from the input signal of the actuator, or in some cases, not be determined at all.

Most of the research related to modal testing of microsystems in liquids was focused on the dynamics of cantilever beams for the atomic force microscopy (AFM) industry. Dynamic AFM shows promising results for the investigation of biological samples in a liquid environment. Multiple excitation methods have been compared for two different cases. The first case focuses on the actuation of the first resonance frequency of AFM cantilevers in liquids and magnetic actuation has been found to be the most effective [25]. The second focuses on the excitation of higher order cantilever modes, magnetostriciton was found to be the most effective [26], although piezoelectric base excitation was left out of consideration.

Modal testing of microsystems in liquids is an emerging research area. Some basic modal tests where done to analyze the dynamic behavior of AFM cantilevers in liquids [25–27, 33, 35, 36, 50, 69, 72, 75–79] but this never reached level 2 of the levels defined by Ewins discussed earlier in this chapter. Also, most of these test setups where built without taking the effect of the dynamic response of the test setup itself on the measurements into account. Research was done on the effects of the liquid cell [32, 49, 50], and in case of piezoelectric base excitation, the effects of the cantilever holder [33–35], however design details on liquid cells and cantilever holders taking their dynamic response into account are not available. Research on the dynamics or microsystems submerged in liquids could greatly benefit from research into the design of modal test equipment.

C

Fluid-structure interaction in microsystems

The submersion of a structure in fluid has important implications on the dynamics of the system. The velocity of the fluid flow near the structure is very low and at the boundary the fluid adheres to the surface of the structure. This results in the so called "added mass" or "virtual mass" effect, schematically represented in figure C.1a. This concept of added mass was first proposed by Friedrich Bessel in 1828 [80] when researching the effect of fluid on the motion of pendula. This effect decreases the resonance frequencies of the modes. The fluid also imposes a resistance to the motion of a submerged structure. This drag force results in added damping. This damping caused by two different damping principles: viscous damping, in which the viscous forces in the liquid dissipate energy, and acoustic radiation damping, in which the energy is radiated away as an acoustic wave traveling through the liquid [53].

An other form of damping common is microsystems is squeeze film damping, shown in figure C.1b. Squeeze film damping arises when two surfaces are approximately parallel to each other separated by a small gap, known as the squeeze film effect. If one of those surfaces moves relative to the other, the fluid is either sucked in, or pumped out, the gap. The resistance the fluid has to this pumping action is the cause of squeeze film damping. The compression and expansion driving the pumping action also imposes a certain stiffness, thus the presence of a squeeze film influences the dynamics of the structure in the fluid near a surface.

These phenomena are nonlinear in nature, however these nonlinear effects were "linearized" in some experiments by the use of random (white noise) excitation [30]. Nonlinear effects of fluid-structure interaction remains a topic of interest [30, 81], especially during tip-sample interactions in atomic force microscopy.

Perhaps the first study of the dynamics of microsystems in liquids was done in 1827 by Robert Brown. He observed the random motion of organic and inorganic micro-scale particles in liquids. The origin of this motion was later, with contributions from Albert Einstein and Jean B. Perrin, discovered to be related to the atomic nature of matter. This motion is now called Brownian motion.

Brownian motion is the motion imposed to a micro-scale sized object by collision of the atoms or molecules of a fluid with the object. The kinetic energy of these atoms or molecules is proportional to the temperature of the fluid. If the object is large compared to the atoms or molecules, meaning that a large number of collisions occur with the object at an instant, the momentum transferred by the random collisions on all sides of the object approach a normal distribution and cancel each other out. It could be said that a certain pressure is action on the object. However, with micro-scale objects, this is not the case. Because the amount of collisions at approximately the same time is far less than with a macro-scale object, the momentum on each side of the micro-scale object is not always normally distributed, resulting in a net momentum, and thus motion, in a certain direction.

The effects of the random Brownian forces can be observed by measuring the vibrations, i.e., the thermal noise spectrum, of a microsystem in liquid. The equipartition theorem states that the energy of each DOF of the system (i.e. each mode) is equal to $\frac{1}{2}k_B T$, where k_B and T denote the Boltzmann constant and the temperature respectively.

A schematic representation of Brownian excitation is depicted in figure C.1c. This form of excitation can be used during the tuning process of the AFM, to measure some basic dynamic characteristics of the cantilever when operating an AFM in liquid [69].

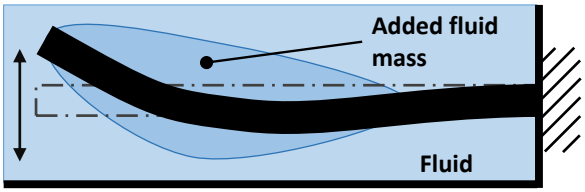

(a) "Added mass" effect: fluid adhering to the submerged structure, increasing its inertia

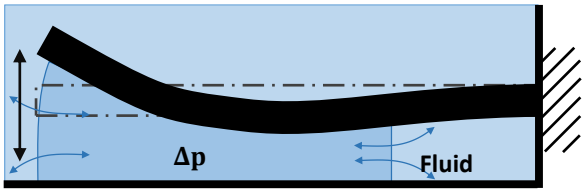

(b) Squeeze film effect: fluid is "pumped" from, and into, a small gap between two surfaces when the surfaces are moving toward, and away from, each other respectively, driven by a pressure difference Δp

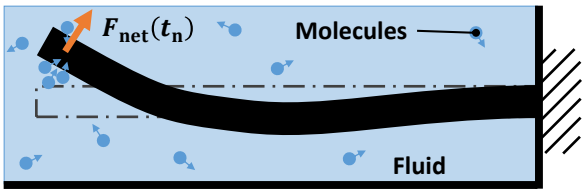

(c) Brownian excitation: structure excited by the random collisions with the molecules, or atoms, of the fluid

Figure C.1: Schematic representation of various fluid-structure interaction phenomena

C.1. Theoretical models

Several analytical models have been proposed [2, 82–84] based on the Navier-Stokes equations, and experimentally verified, to describe the effects of the fluidic added mass and the damping related to the drag of the structure in liquid. These models are only valid for cantilevers however, and the hydrodynamic function is approximated using the hydrodynamic function derived for a sphere[82, 83], an infinity long cylindrical beam [2], or a thin blade[84]. Using the same method, analytical models for other structures such as plates can be derived, given the geometry remains simple.

To achieve a higher accuracy and to enable the modeling of more complex structures, research in finite element models of the fluid-structure interaction was done. A model developed for cantilever beams [85] was examined and a model for plates [86]. Both models encapsulate the structure in a three-dimensional bubble of Navier-Stokes elements describing an incompressible viscous fluid, which is located in a infinite inviscid potential flow domain.

D

Acoustics

Acoustics is the branch of physics that deals with the study of all mechanical waves in gases, liquids, and solids including topics such as vibration, sound, ultrasound and infrasound. The bulk acoustic behavior of fluids can be described by compressional waves. In solids however, in addition to compressional elastic waves, shear waves are present, which makes the analysis more significantly more complicated. Apart from these bulk waves, others waves can be present in domains with boundary conditions. Examples are: capillary waves, flexural waves, Love waves, and Rayleigh wave.

D.1. Impedance Analogy

For one dimensional systems an analogy can be made to electrical systems, where the voltage and the current are replaced by the force and the particle velocity respectively. Following from this, the impedance of the system can be defined as:

$$Z = \frac{F}{\dot{u}} = Az \tag{D.1}$$

where F, $\dot{u}$, z, and A denote the force, particle velocity, specific acoustic impedance, and interface area respectively.

When a acoustic wave coming from one infinite half-space and traveling to the next, the wave reflection and transmission at the boundary can be described by the following coefficients:

$$R_{\mathrm{a}}^{\mathrm{b}} = \frac{z_0 b - z_0 a}{z_0 b + z_0 a} \tag{D.2a}$$

$$T_{\mathrm{a}}^{\mathrm{b}} = \frac{2 z_0 b}{z_0 b + z_0 a} \tag{D.2b}$$

$$z_0 = c_0 \rho_0 \tag{D.2c}$$

where $R_{\mathrm{a}}^{\mathrm{b}}$, $T_{\mathrm{a}}^{\mathrm{b}}$, z_0, c_0 and ρ_0 denote the reflection- and transmission coefficient of the of the wave traveling from material a to b, characteristic acoustic impedance of the material, the speed of sound in the material, and the density of the material respectively. The characteristic acoustic impedance is a material property, measured in Rayl, being $1\,\mathrm{kg/m^2 s}$.

The practice of selecting the characteristic impedances of the materials in such a way that the reflections are minimized is called impedance matching. In practice this done by selecting the impedance of the materials in between the piezo and the target material, to be in between the characteristic impedance of these materials.

D.2. Attenuation

Acoustic attenuation is a measure of the energy loss of sound propagation in media. Most media have material damping and are therefore not ideal media. When sound propagates in such media, there is always

thermal consumption of energy caused by material damping. For inhomogeneous media, besides media viscosity, acoustic scattering is another main reason for removal of acoustic energy. Acoustic attenuation of a plane wave is described by:

$$\frac{p_{\Delta x}}{p_0} = \mathrm{e}^{-\alpha_0 (2\pi f)^2 \Delta x} \tag{D.3}$$

Where $p_{\Delta x}$, p_0, $alpha_0$, f, and Δx denote the pressure amplitude at a certain traveled distance Δx, the initial pressure, the damping of the material, the frequency of the wave, and the traveled distance of the wave until it reached pressure $p_{\Delta x}$. $p_{\Delta x}$ determines the size of the backing material, meaning using a backing material for low frequency transducers would result in very large backing material.

E

Morphological Analysis

The following page in this chapter show the criteria taken into account during the morphological analysis and the back of the envelope calculations made to support the actuator selection.

	Actuation[1]	Influence on dynamics[2]	Bandwidth	Amplitude range [3]	Fabrication	Force detection	Operation[4]	Cost
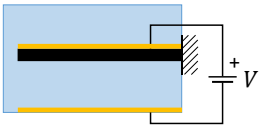	Electrostatic	Eigen frequency shift[5,6]: 10%-30%	300 kHz[7]	3.7 $\left[\frac{\text{N nm}}{\text{m}}\right]$ [7] (water)				
	Integrated piezoelectric	Eigen frequency shift[8]: <30%	1 kHz - 1 GHz[9,10]	325 $\left[\frac{\text{N nm}}{\text{m}}\right]$ [11] (air)				
	Magnetostrictive	Eigen frequency shift[12]: <30%	1 MHz[13]	6.1 $\left[\frac{\text{N nm}}{\text{m}}\right]$ [14] (water)				
	Piezoelectric base	Fluid borne excitation Large base motion[15]	1 kHz - 1 GHz[9,10]	76 $\left[\frac{\text{N nm}}{\text{m}}\right]$ [16] (water)				
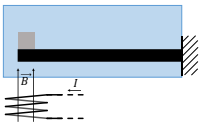	Magnetic	Eigen frequency shift: Coating[12] 20%-30% Particle[17] 20%-70%	1 MHz[18,19]	1.0 $\left[\frac{\text{N nm}}{\text{m}}\right]$ [19] (water)				
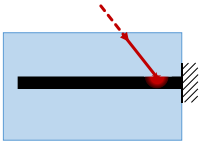	Photo-thermal	Local heating: 1 °C[20] - 30 °C[21,22]	10 MHz[23]	160 $\left[\frac{\text{N nm}}{\text{m}}\right]$ [24] (air, bimorph)				
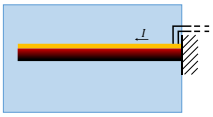	Electro-thermal	Eigen frequency shift[5,12]: 20%-30% Heating[25]: 170 °C	1-30 kHz[25,26]	116 $\left[\frac{\text{N nm}}{\text{m}}\right]$ [25] (air)				
	Shape memory alloy	Eigen frequency shift[5,12]: 20%-30% Heating[27]: 140 °C	<100 Hz[28]					

[1] Operational excitation emitted due to requirements
[2] Influence based on addition of a layer or particle on a silicon nitride beam with dimensions based on Bruker AC-40
With:

$\beta L = 1.875104$	First flexural frequency constant for a cantilever beam, Mechanical Vibrations 5th - S. Rao pag. 726
$\rho_{\text{beam}} = 2810\ \text{kg m}^{-3}$	Density beam http://www.azom.com/properties.aspx?ArticleID=53 (average density)
$\nu_{\text{beam}} = 0.255$	Beam poisson ratio assuming isotropic behavior http://www.azom.com/properties.aspx?ArticleID=53 (average poisson ratio)
$b = 16 \cdot 10^{-6}\ \text{m}$	Cantilever width dimensions based on Bruker AC-40 (BL-AC40TS-C2)
$h = 0.2 \cdot 10^{-6}\ \text{m}$	Cantilever height dimensions based on Bruker AC-40 (BL-AC40TS-C2)
$L = 38 \cdot 10^{-6}\ \text{m}$	Cantilever length dimensions based on Bruker AC-40 (BL-AC40TS-C2)
$f_{\text{flexbeam}} = 110 \cdot 10^{3}\ \text{Hz}$	Cantilever beam's first flexural resonance frequency based on Bruker AC-40 (BL-AC40TS-C2)

Influence on first flexural vibration:

$A_{\text{beam}} = b\ h$, cross-sectional area of silicon nitride beam

$I_{\text{beam}} = \frac{1}{12} b\ h^3$, original second moment of inertia of silicon nitride beam

$E_{\text{beam}} = (2\pi\ f_{\text{beam}})^2\ \frac{\rho_{\text{beam}}\ A_{\text{beam}}\ L^4}{I_{\text{beam}}\ (\beta L)^4}$, Young's modulus of silicon nitride beam based on first natural frequency Bruker AC-40 (BL-AC40TS-C2)

In case of added layer with thickness t, density ρ_{layer}, and Young's modulus E_{layer} :

$A_{\text{layer}} = b\ t$, cross-sectional area of added layer

$y = \frac{E_{\text{beam}}\ A_{\text{beam}}\ \frac{h}{2} + E_{\text{layer}}\ A_{\text{layer}}\ \left(h + \frac{t}{2}\right)}{E_{\text{beam}}\ A_{\text{beam}} + E_{\text{layer}}\ A_{\text{layer}}}$, new neutral axis of the beam

$D_{\text{total}} = E_{\text{beam}} \left(I_{\text{beam}} + A_{\text{beam}} \left(y - \frac{h}{2}\right)^2\right) + E_{\text{layer}} \left(\frac{1}{12} b\ t^3 + A_c \left(h + \frac{t}{2} - y\right)^2\right)$, where $D_{\text{total}} = E_{\text{lumped}}\ I_{\text{lumped}}$, Flexural rigidity of cantilever with added layer

$f_{\text{flexwithlayer}} = \frac{(\beta L)^2}{2\pi} \sqrt{\frac{D_{\text{total}}}{(\rho_{\text{beam}}\ A_{\text{beam}} + \rho_{\text{layer}}\ A_{\text{layer}})\ L^4}}$, first flexural frequency of beam with added layer

$\eta_{\text{layer}} = \frac{f_{\text{flexwithlayer}} - f_{\text{beam}}}{f_{\text{beam}}} \cdot 100\ \%$, influence of added layer on the first flexural natural frequency in percentage

In case of added particle at the end of the beam with characteristic length L_{particle}, and density ρ_{particle}:

$m_{\text{particle}} = \rho_{\text{particle}}\ {L_{\text{particle}}}^3$, mass of particle approximated to be cubicle

$f_{\text{flexwithparticle}} = \frac{1}{2\pi} \sqrt{\frac{K}{M_{\text{effective}} + m_{\text{particle}}}} = \frac{1}{2\pi} \sqrt{\frac{3\ E_b\ \frac{I_{org}}{L^3}}{\frac{3}{(\beta L)^4} \rho_{\text{beam}}\ A_{\text{beam}}\ L + m_{\text{particle}}}}$, where $M_{\text{effective}}$ denotes the effective beam mass as if it where lumped at the end of the beam and K the stiffness of the massless beam determined by Euler–Bernoulli beam theory

$\eta_{\text{particle}} = \frac{f_{\text{flexwithparticle}} - f_{\text{beam}}}{f_{\text{beam}}} \cdot 100\ \%$, influence of added particle on the first flexural natural frequency in percentage

Influence of on first torsional vibration in case of added layer with thickness t, density ρ_{layer}, poisson ratio ν_{layer}, and Young's modulus E_{layer} :

$G_{\text{layer}} = \frac{E_{\text{layer}}}{2\,(1+\nu_{\text{layer}})}$, shear modulus of the added layer

$G_{\text{beam}} = \frac{E_{\text{beam}}}{2\,(1+\nu_{\text{beam}})}$, shear modulus of silicon nitride beam based on first natural frequency Bruker AC-40 (BL-AC40TS-C2) and assuming isotropy

$J_{beam} = b\,h^3\left(\frac{1}{3} - 0.21\,\frac{h}{b}\left(1 - \frac{h^4}{12\,b^4}\right)\right)$, torsion constant rectangular crossection Roark's Formulas for stress & Strain 7th – Young & Budynas pag. 401

$I_{0beam} = \frac{1}{12}\,\rho_{\text{beam}}\,h\,b^3$, polar moment of inertia assuming the cross-sectional area to be a thin plate or a slender rod Engineering Mechanics Dynamics 14th - Hibbeler appendix

$f_{\text{torbeam}} = \frac{(2\,n+1)\,\pi}{2\,\pi}\,\frac{\sqrt{G_{\text{beam}}\,\frac{J_{beam}}{I_{0beam}}}}{2\,L}, \quad n = 1$, Cantilever beam's first torsional resonance frequency Mechanical Vibrations 5th - S. Rao pag. 720

$x = \frac{\frac{\rho_{beam}\,h^2}{2} + \rho_{\text{layer}}\,t\,\left(h + \frac{t}{2}\right)}{\rho_{beam}\,h + \rho_{\text{layer}}\,t}$, cross-sectional center of mass of beam with added layer

$t_{\text{substitute}} = \text{solve}\{G_{\text{layer}}\,((h + t + x)^3 - (h - x)^3) = G_{\text{beam}}\,((h + t_{\text{substitute}} + x)^3 - (h - x)^3)\}$, find the thickness of an added layer of silicon nitride with the same torsional rigidity as the added layer

$J_{\text{total}} = b\,(h + t_{\text{substitute}})^3\left(\frac{1}{3} - 0.21\,\frac{h + t_{\text{substitute}}}{b}\left(1 - \frac{(h + t_{\text{substitute}})^4}{12\,b^4}\right)\right)$, torsion constant rectangular cross-section of beam with layer

$I_{0\text{total}} = \frac{1}{12}\,(\rho_{\text{beam}}\,h + \rho_{\text{layer}}\,t)\,b^3$, polar moment of inertia assuming the cross-sectional area to be a thin plate or a slender rod

$f_{\text{torwithlayer}} = \frac{(2\,n+1)\,\pi}{2\,\pi}\,\frac{\sqrt{G_{\text{beam}}\,\frac{J_{total}}{I_{0total}}}}{2\,L}, \quad n = 1$, first torsional frequency of beam with added layer

$\eta_{\text{torsional}} = \frac{f_{\text{torwithlayer}} - f_{\text{beam}}}{f_{\text{beam}}} \cdot 100\ \%$, influence of added layer on the first torsional natural frequency in percentage

[3] The amplitude range is expressed by the maximum amplitude of the first mode found in literature, modified by the stiffness of the used cantilever. This is not the actual excitation force!

[4] Executing the test procedure, Tuning, post-processing, etc.

[5] Considered properties added layer of gold(Au):

$E_{\text{layer}} = 79 \cdot 10^9\ \text{Pa}$	Young's Modulus of added layer http://www.azom.com/article.aspx?ArticleId=5147
$\rho_{\text{layer}} = 1930\ \text{kg m}^{-3}$	Density of the added layer http://www.azom.com/article.aspx?ArticleId=5147
$t = 0.04 \cdot 10^{-6}\ \text{m}$	Thickness of the added layer based on thickness of applied coating Bruker AC-40 (BL-AC40TS-C2)
$\nu_{layer} = 0.43$	Poisson ratio of the added layer assuming isotropic behavior http://www.azom.com/article.aspx?ArticleId=5147

[6] Considered properties added layer of Indium Tin Oxide(ITO):

$E_{\text{layer}} = 116 \cdot 10^9\ \text{Pa}$	Young's Modulus of added layer http://www.mit.edu/~6.777/matprops/ito.htm
$\rho_{\text{layer}} = 6800\ \text{kg m}^{-3}$	Density of the added layer http://www.mit.edu/~6.777/matprops/ito.htm
$t = 0.02 \cdot 10^{-6}\ \text{m}$	Thickness of the added layer K. Umeda, et al., Appl. Phys. Express, vol. 3, no. 6, p. 65205, Jun. 2010.
$\nu_{layer} = 0.43$	Poisson ratio of the added layer assuming isotropic behavior http://www.mit.edu/~6.777/matprops/ito.htm

[7] K. Umeda, N. Oyabu, K. Kobayashi, Y. Hirata, K. Matsushige, and H. Yamada, "High-Resolution Frequency-Modulation Atomic Force Microscopy in Liquids Using Electrostatic Excitation Method," *Appl. Phys. Express*, vol. 3, no. 6, p. 65205, Jun. 2010. (deflection = 0.5nm, k = 7.4 N/m, medium = water)

[8] Considered properties added layer of zinc oxide(ZnO):

$E_{\text{layer}} = 205 \cdot 10^9\ \text{Pa}$	Young's Modulus of added layer N. Yamamoto, et al., *Adv. Mater. Sci. Eng.*, vol. 2011, no. 1, pp. 1–10, 2011.
$\rho_{\text{layer}} = 5606\ \text{kg m}^{-3}$	Density of the added layer http://www.azom.com/article.aspx?ArticleID=5818
$t = 0.03 \cdot 10^{-6}\ \text{m}$	Thickness of the added layer N. Yamamoto, et al., *Adv. Mater. Sci. Eng.*, vol. 2011, no. 1, pp. 1–10, 2011.
$\nu_{layer} = 0.34$	Poisson ratio of the added layer assuming isotropic behavior H. N. Yoshimura, et al., *Mater. Sci. Forum*, vol. 530–531, pp. 408–413, 2006.

[9] C.-B. Eom and S. Trolier-McKinstry, "Thin-film piezoelectric MEMS," *MRS Bull.*, vol. 37, no. 11, pp. 1007–1017, Nov. 2012.

[10] Measurement Specialties, Inc.,"Piezo Film Sensors Technical Manual", https://www.sparkfun.com/datasheets/Sensors/Flex/MSI-techman.pdf

[11] L. R. Viannie, S. Joshi, G. R. Jayanth, K. Rajanna, and V. Radhakrishna, "AFM cantilever with integrated piezoelectric thin film for micro-actuation," in *2012 IEEE Sensors*, 2012, no. October, pp. 1–4. (deflection = 65 nm, k = 5N/m, medium = air)

[12] Considered properties added layer of ferrous material(Fe-X):

$E_{\text{layer}} = 211 \cdot 10^9\ \text{Pa}$	Young's Modulus of added layer CES Edupack 2016 Material level 2 low alloy steel (average value)
$\rho_{\text{layer}} = 7850\ \text{kg m}^{-3}$	Density of the added layer
$t = 0.05 \cdot 10^{-6}\ \text{m}$	Thickness of the added layer M. Penedo, et al., *Appl. Phys. Lett.*, vol. 95, no. 14, p. 143505, 2009.
$\nu_{layer} = 0.29$	Poisson ratio of the added layer assuming isotropic behavior CES Edupack 2016 Material level 2 low alloy steel (average value)

[13] M. Penedo, A. Raman, S. Hormeño, I. Fernández-Martínez, M. Luna, and F. Briones, "Enhanced efficiency in the excitation of higher modes for atomic force microscopy and mechanical sensors operated in liquids," *Appl. Phys. Lett.*, vol. 105, no. 17, p. 173102, Oct. 2014.

[14] M. Penedo, I. Fernandez-Martinez, J. L. Costa-Kramer, M. Luna, and F. Briones, "Magnetostriction-driven cantilevers for dynamic atomic force microscopy," *Appl. Phys. Lett.*, vol. 95, no. 14, p. 143505, 2009. (deflection = 8 nm, k = 0.76 N/m, medium = water)

[15] D. Kiracofe and A. Raman, "Quantitative force and dissipation measurements in liquids using piezo-excited atomic force microscopy: a unifying theory," *Nanotechnology*, vol. 22, no. 48, p. 485502, Dec. 2011.

[16] C. A. J. Putman, K. O. Van der Werf, B. G. De Grooth, N. F. Van Hulst, and J. Greve, "Tapping mode atomic force microscopy in liquid," *Appl. Phys. Lett.*, vol. 64, no. 18, p. 2454, 1994. (deflection = 200 nm (water), k = 0.38 N/m, medium = water)

[17] Considered properties added particle of ferrous material(Fe-X):

$L_{\text{particle}} = 2 \cdot 10^{-6}\ \text{m}$	Characteristic length of added particle E.-L. Florin, et al., *Rev. Sci. Instrum.*, vol. 65, no. 3, p. 639, 1994.
$\rho_{\text{particle}} = 7850\ \text{kg m}^{-3}$	Density of the added particle CES Edupack 2016 Material level 2 low alloy steel (average value)

[18] M. Penedo, A. Raman, S. Hormeño, I. Fernández-Martínez, M. Luna, and F. Briones, "Enhanced efficiency in the excitation of higher modes for atomic force microscopy and mechanical sensors operated in liquids," *Appl. Phys. Lett.*, vol. 105, no. 17, p. 173102, Oct. 2014.

[19] M. Kageshima, T. Chikamoto, T. Ogawa, Y. Hirata, T. Inoue, Y. Naitoh, Y. J. Li, and Y. Sugawara, "Development of atomic force microscope with wide-band magnetic excitation for study of soft matter dynamics," *Rev. Sci. Instrum.*, vol. 80, no. 2, p. 23705, 2009. (deflection = 10 nm, k = 0.1 N/m, medium = water)

[20] D. Kiracofe, K. Kobayashi, A. Labuda, A. Raman, and H. Yamada, "High efficiency laser photothermal excitation of microcantilever vibrations in air and liquids," *Rev. Sci. Instrum.*, vol. 82, no. 1, p. 13702, 2011.

[21] D. Ramos, J. Tamayo, J. Mertens, and M. Calleja, "Photothermal excitation of microcantilevers in liquids," *J. Appl. Phys.*, vol. 99, no. 12, p. 124904, 2006.

[22] J. S. Nabeth, S. Chigullapalli, and A. A. Alexeenko, "What Determines Knudsen Force at the Microscale," in *AIP Conference Proceedings*, 2011, vol. 1333, no. PART 1, pp. 754–759.

[23] S. Nishida, D. Kobayashi, H. Kawakatsu, and Y. Nishimori, "Photothermal excitation of a single-crystalline silicon cantilever for higher vibration modes in liquid," *J. Vac. Sci. Technol. B Microelectron. Nanom. Struct.*, vol. 27, no. 2, p. 964, 2009.

[24] N. Umeda, "Scanning attractive force microscope using photothermal vibration," *J. Vac. Sci. Technol. B Microelectron. Nanom. Struct.*, vol. 9, no. 2, p. 1318, Mar. 1991. (16 nm, k = 10 N/m, medium = air)

[25] J. Lee and W. P. King, "Microcantilever actuation via periodic internal heating," *Rev. Sci. Instrum.*, vol. 78, no. 12, p. 126102, 2007. (deflection = 484 nm, k = 0.24 N/m, medium = air)

[26] J. J. Allen, *Micro Electro Mechanical System Design*. CRC Press, 2005.

[27] T. Kniknie, Y. Bellouard, E. Homburg, H. Nijmeijer, X. Wang, and J. J. Vlassak, "On the use of shape memory alloy thin films to tune the dynamic response of micro-cantilevers," *J. Micromechanics Microengineering*, vol. 20, no. 1, p. 15039, Jan. 2010.

[28] Y. Bellouard, "Shape memory alloys for microsystems: A review from a material research perspective," *Mater. Sci. Eng. A*, vol. 481–482, no. 1–2 C, pp. 582–589, May 2008.

	Mounting[1]	Damping[2]	Robustness[3]	Fabrication[4]	Operation[5]	Cost[6]
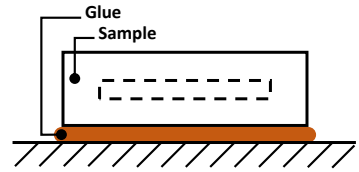	Glue					
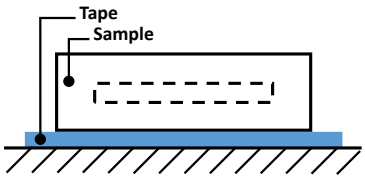	Double sided tape					
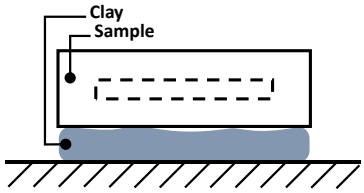	Clay					
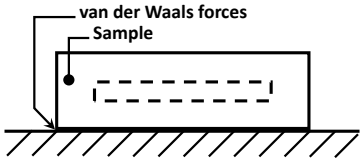	Wringing[7]					
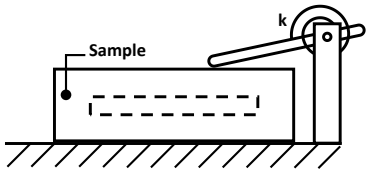	Spring					
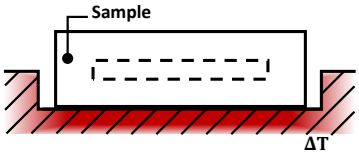	Temperature preload					

[1] Vacuum mounting omitted due to requirements for vacuum environment

[2] Especially in a liquid environment, where quality factors are already low, an increase in damping from the mounting would lower the quality factors even more. Energy loss through the mounting should be reduced

[3] The robustness of the mounting denotes how quickly the sample will be displaced by a disturbance, e.g., when bumping into the sample after mounting, or an initial flow of liquid when flooding the cell

[4] The difficulty in fabrication. Some components might be easily fabrication because automated fabrication techniques are required (CNC, laser cutting, lithography), the processes are generally more expensive though, this will be reflected in the **cost** criteria.

[5] Sample preparation, switching samples, etc.

[6] Initial (fabrication) cost, cost per sample (fabrication), maintenance

[7] https://en.wikipedia.org/wiki/Gauge_block#Wringing (*NL: Eindmaat*)

F

Design details

F.1. Material Selection

F.1.1. Back Mass

The back mass material is chosen to be as heavy as possible for a certain length. As shown in equation F.1 and F.2, the mass of the back mass is proportional to its acoustic impedance. Since length does not only influence mass, but also resonance frequency. The candidate materials are shown in figure F.1. Stainless steel is chosen as material due to its relatively low cost compared to its acoustic impedance, and because its a common used material in machine shops.

$$L = \frac{\lambda}{2} = \frac{c}{2f} \tag{F.1}$$

$$\tilde{m} = \rho L = \frac{z}{2f} \propto z \tag{F.2}$$

F.1.2. Acoustic Horn

For optimal energy transfer the acoustic impedance of the material for the acoustic horn should be in between the piezo (35 MRayl) and silicon. The candidate materials, being selected on their chemical resistance to fresh water, are shown in figure F.2. Based on this figure, the cost and the chemical resistance of the materials, Titanium has been chosen as material for the acoustic horn.

F.1.3. Environment Chamber

The initial material selection was done on level 2 of CESEdupack with extended durability properties to find suitable materials for further investigation. An excellent chemical resistance to common weak acids, weak alkalis, aqueous solutions and disinfectants is required. Furthermore a service temperature range from $-10\,^{\circ}\mathrm{C}$ to $200\,^{\circ}\mathrm{C}$ is required to allow the possibility of heating the environment chamber, also known as bake-out (temperatures typically between $150\,^{\circ}\mathrm{C}$ to $300\,^{\circ}\mathrm{C}$ [1]), allowing the system to achieve a higher vacuum at a faster rate. The materials where filtered by the requirements shown in table F.1 and F.2. The resultant materials are shown in table F.3.

These materials are not all suitable though. Ceramic foam is permeable, which makes it unsuitable to contain liquid or vacuum. In addition, the ceramics will be difficult to manufacture. Which leaves stainless steel, PTFE and gold. Due to its chemical inertia gold would be the ideal material, it is rather expensive however. A way to limit the cost would be to gold plate another material which would provide structural integrity and has a low permeability. The choice between stainless steel and PTFE depends on the priority of the user. If the setup, will mainly be used for experiments with different liquid chemicals, PTFE or a similar polymer will be favorable over stainless steel due to its high chemical resistance to an extreme wide variety of chemicals. If however the setup will mainly be used for experiments in vacuum and with different kinds of gasses, a type of stainless steel will be a better option, due to its low outgassing, permeability and excellent chemical resistance to pure oxygen. Figure F.3 shows the acoustic impedance of the different material candidates. The

[1] CERN Design rules for vacuum chambers

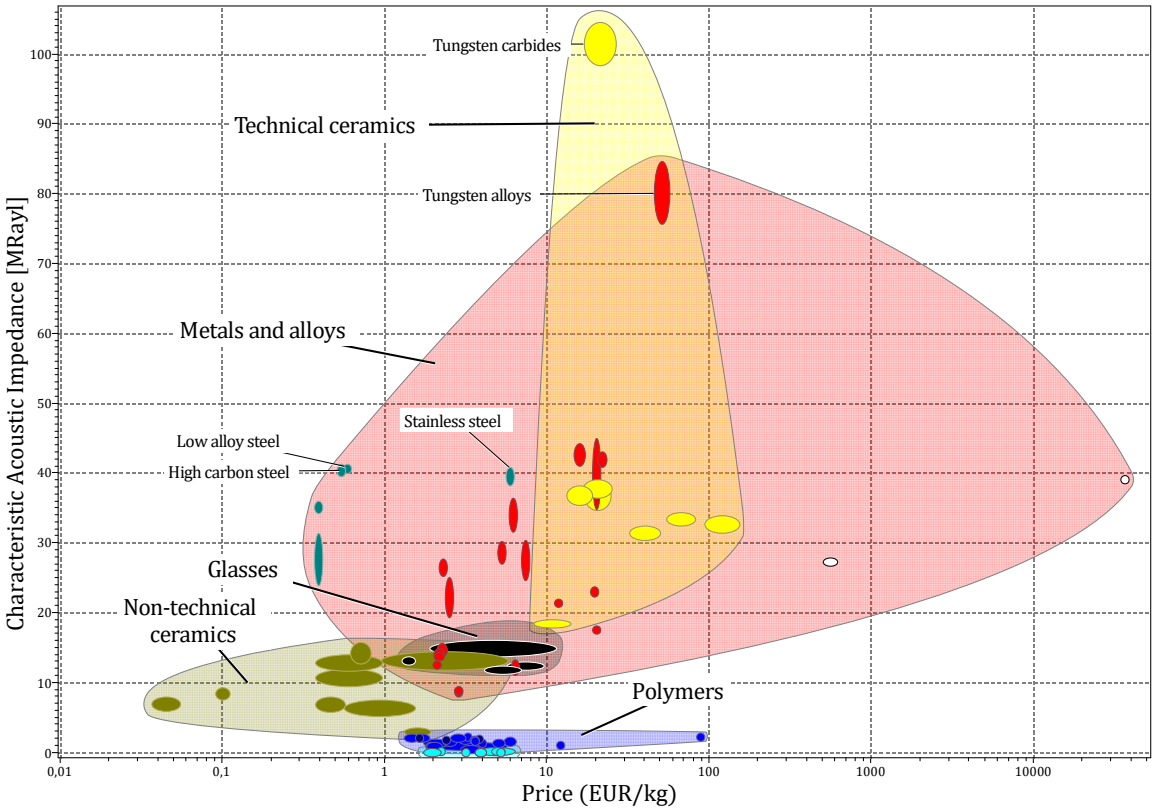

Figure F.1: Acoustic impedance back mass candidate materials

blue dashed line indicated the acoustic impedance of water (1,5 MRayl). From these results PTFE is chosen as the material for the environment chamber because of its excellent chemical resistance, relatively low outgassing (compared to other polymers) and its characteristic impedance close to that of water, which allows it to absorb vibrations from the liquid.

F.2. Required Vacuum Level

Figure F.4 shows the influence of pressure on the damping of a system immersed in air. At ambient pressure and above the dominant damping is determined by viscous damping. When lowering the pressure the damping slowly decreases until the first critical pressure. Here the damping is determined by molecular dynamics, also known as free molecular flow. When the pressure is decreased further the damping significantly drops until the second critical point is reached. At this point free molecular damping can be neglected and material damping is the dominant damping in the system. This critical value is a function of the size, shape, and mode of the resonator. The critical pressure has been measured to range from 10^{-2} mbar to 10^{2} mbar for microsystems [53]. The minimum vacuum level is therefor chosen 10^{-3} mbar to be sure the system operates in the structural damping regime.

F.3. Liquid Cell Resonances

To evaluate the effect of the acoustic impedance match of PTFE to the water in the liquid cell on the liquid cell response a FEA was done. Figure F.5a shows the liquid cell as modelled. An impedance boundary was imposed on all boundaries except the top. Assuming that the impedance mismatch between glass and water is so high this can be modelled as a hard wall. Figure F.5b shows an bar chart of the found damped natural frequencies and quality factors of the liquid cell assuming each mode to behave as a 1 DOF oscillator described by the universal oscillator equation:

$$-\frac{\omega}{\omega_n}q + 2j\zeta\frac{\omega}{\omega_n} + 1 = 0$$

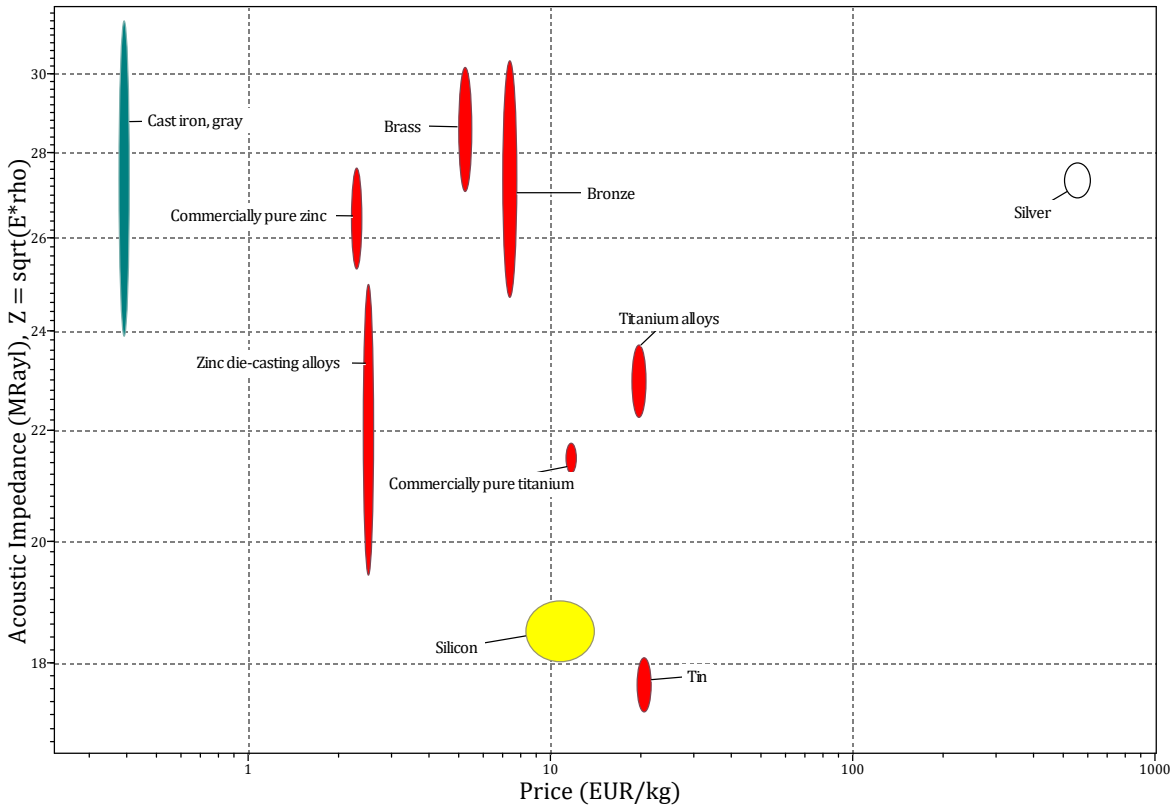

Figure F.2: Acoustic impedance acoustic horn candidate materials

where ω, ω_n, ζ denote the frequency, the undamped natural frequency, and the damping respectively and assuming the vibration response $q = \hat{q}e^{j\omega t}$. From the solution to this equation, the damped natural frequency and quality factor can be derived. $f_{\text{damped}} = f_n\sqrt{1-\zeta^2} = \Re\{f_{\text{eig}}\}$, and $Q = \frac{1}{2\zeta} = \frac{\sqrt{\Re\{f_{\text{eig}}\}^2+\Im\{f_{\text{eig}}\}^2}}{2\Im\{f_{\text{eig}}\}}$. It is shown in figure F.5b that, although there are a large number of eigenfrequencies, they are heavily damped. This analysis assumes the vibrations transferred from the liquid to be fully damped out in the PTFE environment chamber.

F.4. Optics

F.4.1. Optical System

Figure F.6 shows the optical system of the setup. The effect of the environment chamber on the optics of the laser Doppler vibrometer is calculated using geometrical ray optics. The involved parameters shown in figure F.6, and table F.4[2], and F.5[3] are: $M_{\text{objective}}$, $s_{\text{objective}}$, D, $FOV_{\text{objective}}$, n_{air}, n_{glass}, n_{medium}, t, and h denote the objective lens magnification, the working distance in air, the objective lens diameter, the objective field of view, the refractive index air, the refractive index optical window, the refractive index medium, the optical window thickness, and the chamber height respectively. The results are shown in table F.6. s, A_{covered}, and M denote the new working distance, the area covered by the top flange, and the new magnification.

F.4.2. Optical Window Thickness

The minimum thickness of the optical window can be derived from Roark's formula for deflection of a round clamped plate[4] (equation F.3). Figure F.7 shows a schematic of the situation.

[2] Mitutoyo Microscope Units and Objectives Catalog no. E14020
[3] `http://www.engineeringtoolbox.com/refractive-index-d_1264.html`
[4] Roark Table 11.2, page 457, and Roark Table 11.2-10b, where $r_0 = 0$, page 488

Table F.1: Chemical resistance requirements

Chemical	**Durability**
Water(fresh)	Excellent
Water(salt)	Excellent
Wine	Excellent
Acetic acid (10%) (vinegar), CH3COOH	Excellent
Acetic acid (glacial), CH3COOH	Acceptable, Excellent
Citric acid (10%), HOOCCH2COOH(OH)CH2COOH	Excellent
Hydrochloric acid (10%), HCl	Excellent
Nitric acid (10%), HNO3	Excellent
Phosphoric acid (10%), H3PO4	Excellent
Sulfuric acid (10%), H2SO4	Acceptable, Excellent
Sodium hydroxide (10%) (caustic soda), NaOH	Excellent
Sodium hydroxide (60%) (caustic soda), NaOH	Acceptable, Excellent
Petroleum (gasoline)	Excellent
Turpentine, C10H16	Acceptable, Excellent
Vegetable oils	Excellent
White spirit (Stottard solvent)	Excellent
Acetaldehyde (Ethanal), CH3CHO	Excellent
Acetone (propanone) CH3COCH3	Excellent
Ethyl alcohol (Ethanol), CH3CH2OH	Excellent
Formaldehyde (40%)(Methanal), CH2O	Acceptable, Excellent
Glycerol (Glycerin), HOCH2CH2CH2(OH)CH2OH	Excellent
Methyl alcohol (Methanol), CH3OH	Excellent
Chlorine gas (dry), Cl2	Excellent
Oxygen gas, O2	Acceptable, Excellent

Table F.2: Thermal requirements

Temperature	**Range**
Service temperature	−10 °C to 200 °C

$$t_{\min} = a\sqrt{\frac{3\Delta pK}{4\sigma_{\max}}} \tag{F.3}$$

where $t_{\min}$, a, Δp, K, and $\sigma_{\max}$ denote the minimum window thickness, the window radius, the pressure load, the safety factor, and the maximum allowable stress in material[5].

F.5. Influence of Glue on the Acoustic Impedance

The glue with which the actuator components are glued together also influences the energy transfer of actuator. If the glue layer was significantly thick the reflection and transmission coefficients as discussed in chapter D hold. However, the closer the thickness of the glue gets to a infinity thin layer, the more this theory falls apart. The influence of the glue on the impedance of the total system is dependent on the thickness of the glue relatively to the wavelength of the wave being transferred through the glue. This relation can be described with the equation for the input impedance of transmission line [87–89]:

$$\frac{z_{\text{load}}}{z_{0\text{titanium}}} = \frac{z_{0\text{glue}}}{z_{0\text{titanium}}} \frac{z_{0\text{titanium}} + z_{0\text{glue}} \tanh\left(2\pi \frac{t}{\lambda_{\text{glue@1 MHz}}}\right)}{z_{0\text{glue}} + z_{0\text{titanium}} \tanh\left(2\pi \frac{t}{\lambda_{\text{glue@1 MHz}}}\right)} \tag{F.4}$$

where z_{load}, $z_{0\text{titanium}}$ and $z_{0\text{glue}}$, $\frac{t}{\lambda_{\text{glue@1 MHz}}}$ denote the impedance of the glue and titanium acoustic horn lumped together, the characteristic impedance of the titanium and glue, and the thickness of the glue layer

[5] `http://glassproperties.com/references/MechPropHandouts.pdf` 31-08-2017, slide 3

Table F.3: Results of the material selection of the environment chamber

Material	**Acoustic Impedance (MRayl)**
Polytetrafluoroethylene (Teflon, PTFE)	0,931 - 1,09
Ceramic foam	0,953 - 1,44
Brick	5,2 - 7,48
Sandstone	5,82 - 7,84
Concrete	6,04 - 7,84
Cement	7,66 - 9,21
Limestone	9,49 - 11,9
Borosilicate glass	11,7 - 12,1
Marble	11,8 - 14
Granite	11,9 - 14,4
Silica glass	12,2 - 12,8
Slate	12,8 - 15,8
Soda-lime glass	12,9 - 13,3
Glass ceramic	13,9 - 16,1
Silicon	18 - 19
Bronze	24,7 - 30,3
Brass	27,1 - 30,2
Silicon nitride	30,4 - 32,4
Aluminum nitride	31,5 - 33,9
Copper	31,6 - 36,4
Boron carbide	32,5 - 34,3
Zirconia	34,7 - 38,8
Nickel-based superalloys	35 - 44,9
Silicon carbide	35,5 - 38,1
Alumina	36,5 - 39
Stainless steel	38,3 - 40,8
Gold	38,6 - 39,6
Nickel-chromium alloys	41 - 43
Nickel	41,1 - 44,2
Tungsten carbides	98,5 - 105

Table F.4: Objective lens parameters

$M_{\text{objective}}$ (mm)	5	20	100
$s_{\text{objective}}$ (mm)	37.5	20	13
D (mm)	23	24.4	22
$FOV_{\text{objective}}$ (mm)	1.28	0.32	0.06

Table F.5: Refractive index media

Medium	Refractive index
Glass	1.5
Air	1.000293
Vacuum	1.00
Water	1.333

normalized by the wavelength at 1 MHz respectively. This equation is shown in figure F.8b. To evaluate the influence of the glue in practice the thickness of two samples where measured, found in table F.7. Their influence, as shown in figure F.8b is negligible.

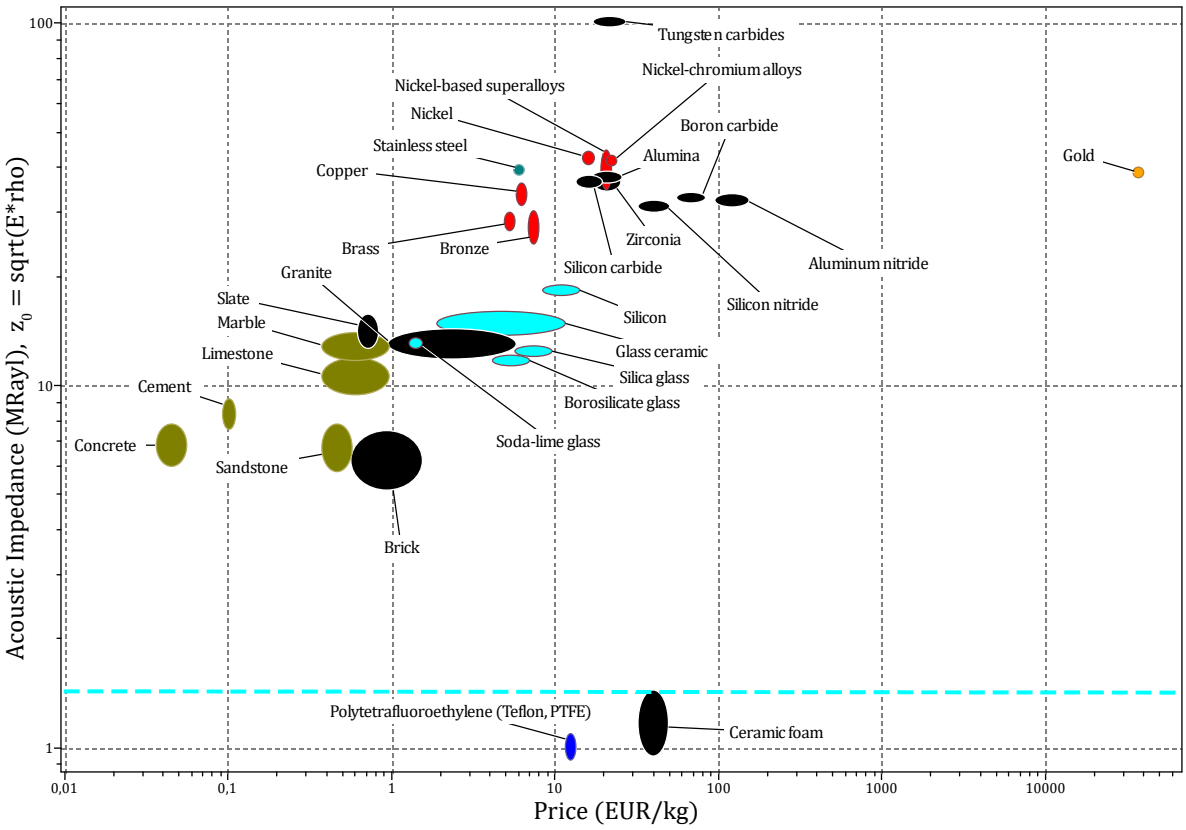

Figure F.3: Acoustic impedance environment chamber candidate materials

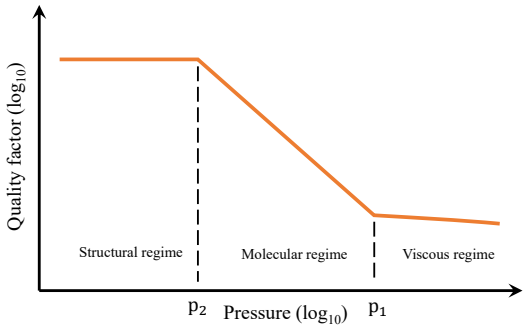

Figure F.4: Influence of pressure on damping from the medium

Table F.6: Results of optical analysis

Objective		5x			20x			100x	
n_{medium}	Air	Vacuum	Water	Air	Vacuum	Water	Air	Vacuum	Water
s (mm)	37.89	37.89	38.80	20.43	20.43	21.48	13.48	13.48	14.66
A_{covered} (%)	0.00	0.00	0.00	18.27	18.28	10.53	31.40	31.41	22.84
M	5.05	5.05	5.16	20.37	20.36	21.20	102.79	102.79	109.04

Table F.7: Measured layer thickness of the conductive glue

Sample	Bare (mm) (± 0.002)	Glued (mm)(± 0.002)	Glue thickness(µm)(± 4)
1	15.225	15.241	16
2	14.933	14.951	18

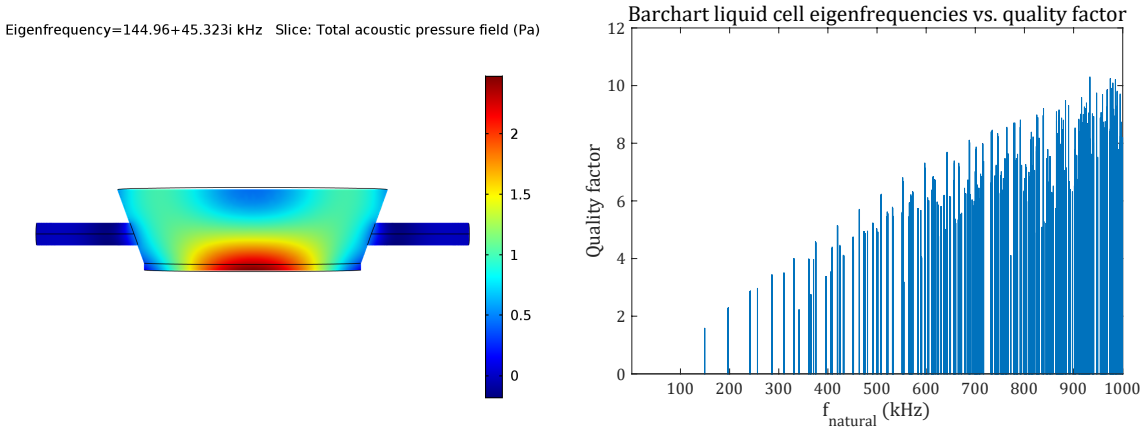

(a) First mode of the liquid cell in the range 1 kHz to 1000 kHz

(b) Bar chart showing the damped natural frequencies and corresponing quality factors of the liquid cell

Figure E.5: Determining the influence of PTFE on the modes of the liquid cell

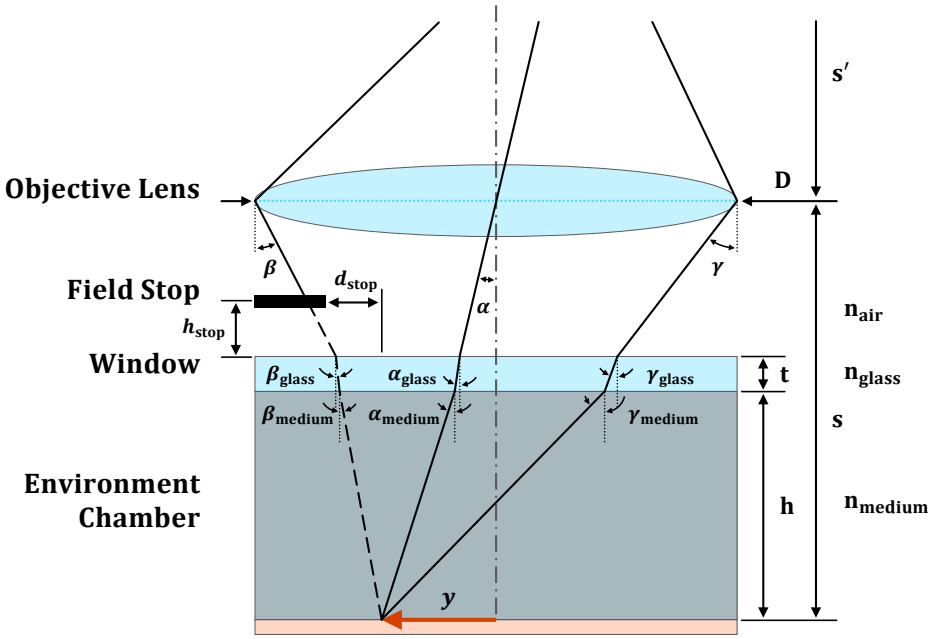

Figure E.6: Ray path analysis of the optical system

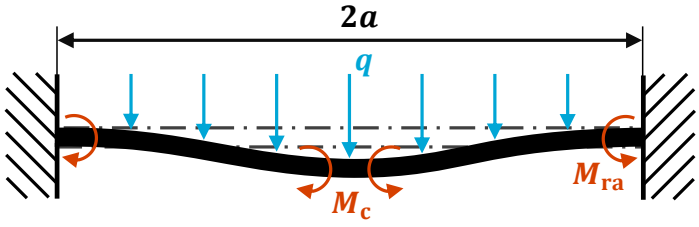

Figure E.7: Maximum allowed deflection of optical window

(a) Samples used to estimate the thickness of the glue

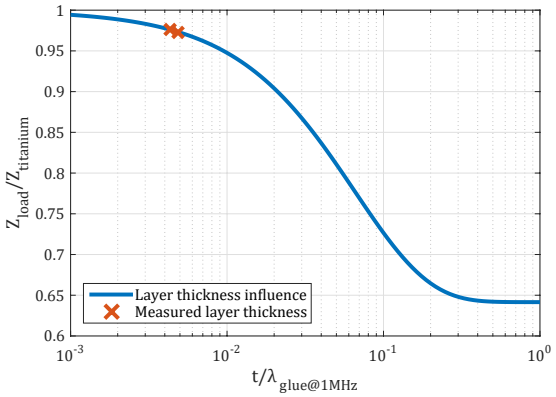

(b) Graph showing the influence of glue layer thickness t, normalized to the wavelength at 1 MHz, on the acoustic impedance

Figure F.8: Determining the influence of the glue

G

Additional Measurements

Figure G.1 shows the response of the CONT cantilever measured with the Polytec.

G.1. Additional Measurement Data Contact Mode AFM Probe (CONT)

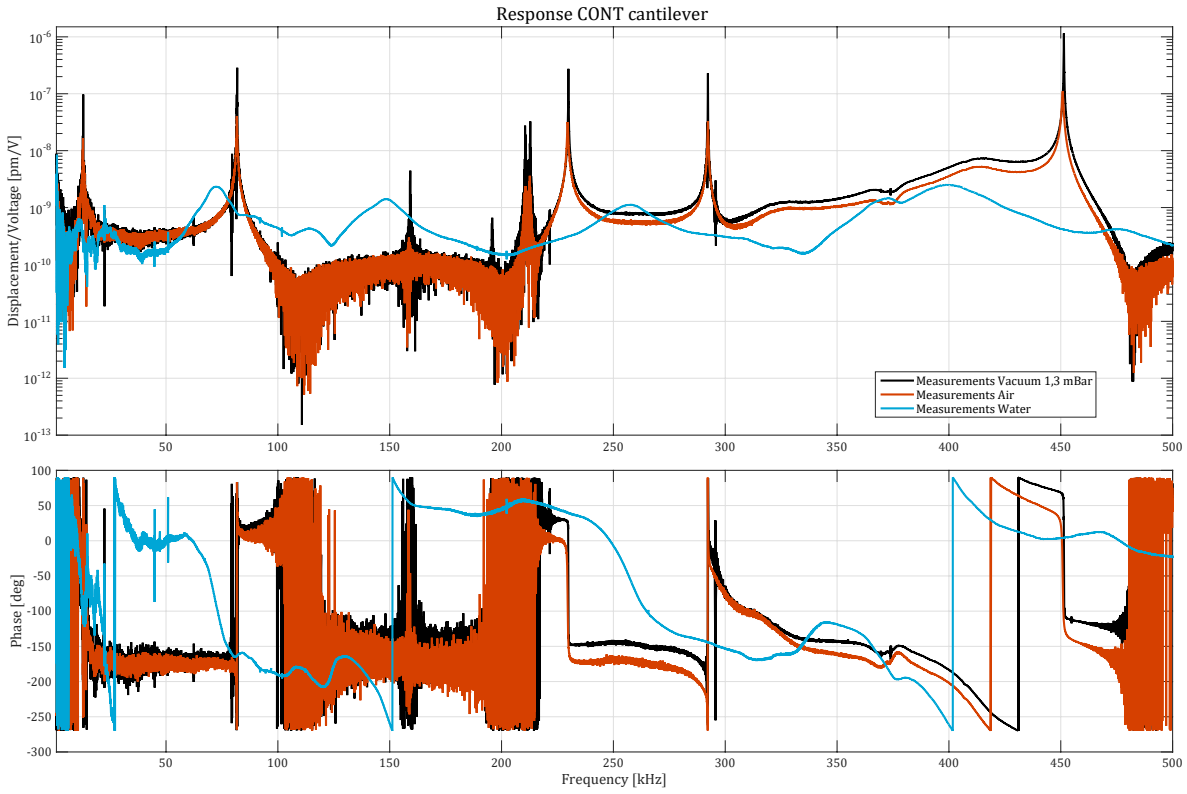

Figure G.1: Frequency response of the CONT cantilever measured with the Polytec system

Bibliography

[1] Cornelis A. Van Eysden and John E Sader. Resonant frequencies of a rectangular cantilever beam immersed in a fluid. *Journal of Applied Physics*, 100(11):114916, 2006.

[2] John Elie Sader. Frequency response of cantilever beams immersed in viscous fluids with applications to the atomic force microscope. *Journal of Applied Physics*, 84(1), 1998.

[3] Christopher P. Green and John E. Sader. Torsional frequency response of cantilever beams immersed in viscous fluids with applications to the atomic force microscope. *Journal of Applied Physics*, 92(10), 2002.

[4] Vytautas Ostasevicius and Rolanas Dauksevicius. *Microsystems Dynamics*, volume 44 of *Intelligent Systems, Control and Automation: Science and Engineering*. Springer Netherlands, Dordrecht, 2011.

[5] Mohammad I. Younis, Fadi Alsaleem, and Daniel Jordy. The response of clamped–clamped microbeams under mechanical shock. *International Journal of Non-Linear Mechanics*, 42(4):643–657, may 2007.

[6] R.M. Lin and W.J. Wang. Structural dynamics of microsystems—current state of research and future directions. *Mechanical Systems and Signal Processing*, 20(5):1015–1043, jul 2006.

[7] Tomas R. Rodrıiguez and Ricardo Garcia. Compositional mapping of surfaces in atomic force microscopy by excitation of the second normal mode of the microcantilever. *Applied Physics Letters*, 84(3):449, 2004.

[8] Sudipta Basak and Arvind Raman. Dynamics of tapping mode atomic force microscopy in liquids: Theory and experiments. *Applied Physics Letters*, 91(6):064107, 2007.

[9] Xin Xu, John Melcher, Sudipta Basak, Ron Reifenberger, and Arvind Raman. Compositional contrast of biological materials in liquids using the momentary excitation of higher eigenmodes in dynamic atomic force microscopy. *Physical Review Letters*, 102(6):13–16, 2009.

[10] Xin Xu, John Melcher, and Arvind Raman. Accurate force spectroscopy in tapping mode atomic force microscopy in liquids. *Physical Review B*, 81(3):035407, jan 2010.

[11] Daniel Kiracofe and Arvind Raman. Microcantilever dynamics in liquid environment dynamic atomic force microscopy when using higher-order cantilever eigenmodes. *Journal of Applied Physics*, 108(3):034320, 2010.

[12] Jose R. Lozano and Ricardo Garcia. Theory of Multifrequency Atomic Force Microscopy. *Physical Review Letters*, 100(7):076102, feb 2008.

[13] a. Raman, S. Trigueros, A. Cartagena, a. P. Z. Stevenson, M. Susilo, E. Nauman, and S. Antoranz Contera. Mapping nanomechanical properties of live cells using multi-harmonic atomic force microscopy. *Nature Nanotechnology*, 6(12):809–814, nov 2011.

[14] Ricardo Garcia and Elena T. Herruzo. The emergence of multifrequency force microscopy. *Nature Nanotechnology*, 7(4):217–226, apr 2012.

[15] K.S. Karvinen and S.O.R. Moheimani. Control of the higher eigenmodes of a microcantilever: Applications in atomic force microscopy. *Ultramicroscopy*, 137:66–71, feb 2014.

[16] Benjamin A Bircher, Roger Krenger, and Thomas Braun. Influence of squeeze-film damping on higher-mode microcantilever vibrations in liquid. *EPJ Techniques and Instrumentation*, 1(1):10, dec 2014.

[17] Angelica P. Davila, Jaesung Jang, Amit K. Gupta, Tom Walter, Arthur Aronson, and Rashid Bashir. Microresonator mass sensors for detection of Bacillus anthracis Sterne spores in air and water. *Biosensors and Bioelectronics*, 22(12):3028–3035, jun 2007.

[18] Murali Krishna Ghatkesar, Viola Barwich, Thomas Braun, Jean-Pierre Ramseyer, Christoph Gerber, Martin Hegner, Hans Peter Lang, Ute Drechsler, and Michel Despont. Higher modes of vibration increase mass sensitivity in nanomechanical microcantilevers. *Nanotechnology*, 18(44):445502, nov 2007.

[19] I. Stachiv, A. I. Fedorchenko, and Y.-L. Chen. Mass detection by means of the vibrating nanomechanical resonators. *Applied Physics Letters*, 100(9):093110, 2012.

[20] Murali Krishna Ghatkesar, Ekaterina Rakhmatullina, Hans-Peter Lang, Christoph Gerber, Martin Hegner, and Thomas Braun. Multi-parameter microcantilever sensor for comprehensive characterization of Newtonian fluids. *Sensors and Actuators B: Chemical*, 135(1):133–138, dec 2008.

[21] J Vázquez, M a Rivera, J Hernando, and J L Sánchez-Rojas. Dynamic response of low aspect ratio piezoelectric microcantilevers actuated in different liquid environments. *Journal of Micromechanics and Microengineering*, 19(1):015020, jan 2009.

[22] Benjamin A Bircher, Luc Duempelmann, Kasper Renggli, Hans Peter Lang, Christoph Gerber, Nico Bruns, and Thomas Braun. Real-Time Viscosity and Mass Density Sensors Requiring Microliter Sample Volume Based on Nanomechanical Resonators. *Analytical Chemistry*, 85(18):8676–8683, sep 2013.

[23] Seonghwan Kim, Kenneth D Kihm, and Thomas Thundat. Fluidic applications for atomic force microscopy (AFM) with microcantilever sensors. *Experiments in Fluids*, 48(5):721–736, may 2010.

[24] D. J. Ewins. *Modal Testing: theory, practice and applications*. 2 edition, 2000.

[25] Xin Xu and Arvind Raman. Comparative dynamics of magnetically, acoustically, and Brownian motion driven microcantilevers in liquids. *Journal of Applied Physics*, 102(3):034303, 2007.

[26] M. Penedo, A. Raman, S. Hormeño, I. Fernández-Martínez, M. Luna, and F. Briones. Enhanced efficiency in the excitation of higher modes for atomic force microscopy and mechanical sensors operated in liquids. *Applied Physics Letters*, 105(17):173102, oct 2014.

[27] Ken-ichi Umeda, Noriaki Oyabu, Kei Kobayashi, Yoshiki Hirata, Kazumi Matsushige, and Hirofumi Yamada. High-Resolution Frequency-Modulation Atomic Force Microscopy in Liquids Using Electrostatic Excitation Method. *Applied Physics Express*, 3(6):065205, jun 2010.

[28] T Sulchek, R Hsieh, J D Adams, S C Minne, C F Quate, and D M Adderton. High-speed atomic force microscopy in liquid. *Review of Scientific Instruments*, 71(5):2097, 2000.

[29] M. Penedo, I. Fernandez-Martinez, J. L. Costa-Kramer, M. Luna, and F. Briones. Magnetostriction-driven cantilevers for dynamic atomic force microscopy. *Applied Physics Letters*, 95(14):143505, 2009.

[30] DS Epp, OB Ozdoganlar, and PM Chaplya. A base excitation test facility for dynamic testing of microsystems. *Proc. of 22nd Int. Modal Analysis Conf.(IMAC)*, (Ldv), 2004.

[31] Wen-Pin Lai and Weileun Fang. Novel bulk acoustic wave hammer to determinate the dynamic response of microstructures using pulsed broad bandwidth ultrasonic transducers. *Sensors and Actuators A: Physical*, 96(1):43–52, jan 2001.

[32] Constant A. J. Putman, Kees O. Van der Werf, Bart G. De Grooth, Niek F. Van Hulst, and Jan Greve. Tapping mode atomic force microscopy in liquid. *Applied Physics Letters*, 64(18):2454, 1994.

[33] Hitoshi Asakawa and Takeshi Fukuma. Spurious-free cantilever excitation in liquid by piezoactuator with flexure drive mechanism. *Review of Scientific Instruments*, 80(10):103703, 2009.

[34] C. Carrasco, P. Ares, P. J. de Pablo, and J. Gomez-Herrero. Cutting down the forest of peaks in acoustic dynamic atomic force microscopy in liquid. *Review of Scientific Instruments*, 79(12):126106, 2008.

[35] Abdelhamid Maali, Cedric Hurth, Touria Cohen-Bouhacina, Geerard Couturier, and Jean-Pierre Aime. Improved acoustic excitation of atomic force microscope cantilevers in liquids. *Applied Physics Letters*, 88(16):163504, 2006.

[36] F. L. Degertekin, B. Hadimioglu, T. Sulchek, and C. F. Quate. Actuation and characterization of atomic force microscope cantilevers in fluids by acoustic radiation pressure. *Applied Physics Letters*, 78(11):1628, 2001.

[37] A. E. Siegman. *Lasers*. University Science Books, 1986.

[38] C J Wilson and D B Bogy. Experimental Modal Analysis of a Suspension Assembly Loaded on a Rotating Disk. *Journal of Vibration and Acoustics*, 116(1):85, 1994.

[39] Wenhai Han, S M Lindsay, and Tianwei Jing. A magnetically driven oscillating probe microscope for operation in liquids. *Applied Physics Letters*, 69(26):4111, 1996.

[40] N. Umeda. Scanning attractive force microscope using photothermal vibration. *Journal of Vacuum Science & Technology B: Microelectronics and Nanometer Structures*, 9(2):1318, mar 1991.

[41] Daniel Kiracofe, Kei Kobayashi, Aleksander Labuda, Arvind Raman, and Hirofumi Yamada. High efficiency laser photothermal excitation of microcantilever vibrations in air and liquids. *Review of Scientific Instruments*, 82(1):013702, 2011.

[42] Arturas Ulcinas, Loren M. Picco, Monica Berry, J.K. Heinrich Horber, and Mervyn J. Miles. Detection and photothermal actuation of microcantilever oscillations in air and liquid using a modified DVD optical pickup. *Sensors and Actuators A: Physical*, 248:6–9, sep 2016.

[43] Jungchul Lee and William P. King. Microcantilever actuation via periodic internal heating. *Review of Scientific Instruments*, 78(12):126102, 2007.

[44] Jeffrey L. Hutter and John Bechhoefer. Calibration of atomic-force microscope tips. *Review of Scientific Instruments*, 64(7):1868, 1993.

[45] H J Butt and M Jaschke. Calculation of thermal noise in atomic force microscopy. *Nanotechnology*, 6(1):1–7, jan 1995.

[46] Jose R Lozano, Daniel Kiracofe, John Melcher, Ricardo Garcia, and Arvind Raman. Calibration of higher eigenmode spring constants of atomic force microscope cantilevers. *Nanotechnology*, 21(46):465502, nov 2010.

[47] Yuan-Fang Chou and Li-Chung Wang. On the Modal Testing of Microstructures: Its Theoretical Approach and Experimental Setup. *Journal of Vibration and Acoustics*, 123(1):104, 2001.

[48] N.F. Smith, D.M. Tanner, S.E. Swanson, and S.L. Miller. Non-destructive resonant frequency measurement on MEMS actuators. In *2001 IEEE International Reliability Physics Symposium Proceedings. 39th Annual (Cat. No.00CH37167)*, volume 2001-Janua, pages 99–105. IEEE, 2001.

[49] Ramin Motamedi and Paula M. Wood-Adams. Influence of Fluid Cell Design on the Frequency Response of AFM Microcantilevers in Liquid Media. *Sensors*, 8(9):5927–5941, sep 2008.

[50] J. Kokavecz and A. Mechler. Investigation of fluid cell resonances in intermittent contact mode atomic force microscopy. *Applied Physics Letters*, 91(2):023113, 2007.

[51] Dennis M. Freeman. Computer Microvision for MicroElectroMechanical Systems (MEMS). Technical Report November, Massachusetts Institute of Technology, 2003.

[52] Jaap Kokorian, Federico Buja, and Willem Merlijn van Spengen. In-Plane Displacement Detection With Picometer Accuracy on a Conventional Microscope. *Journal of Microelectromechanical Systems*, 24(3):618–625, jun 2015.

[53] Surabhi Joshi, Sherman Hung, and Srikar Vengallatore. Design strategies for controlling damping in micromechanical and nanomechanical resonators. *EPJ Techniques and Instrumentation*, 1(1):5, dec 2014.

[54] K.F. Graff. Wave Motion in Elastic Solids, 1991.

[55] K. Nakamura. *Ultrasonic transducers*. Woodhead Publishing Limited, 2012.

[56] Peter Eaton and Paul West. *Atomic Force Microscopy*. Oxford University Press, mar 2010.

[57] Gary X. Li and Henry G. Hughes. Review of Viscous Damping in Micromachined Structures. Number August 2000, pages 30–46, aug 2000.

[58] Minhang Bao and Heng Yang. Squeeze film air damping in MEMS. *Sensors and Actuators A: Physical*, 136(1):3–27, may 2007.

[59] V Ruiz-Díez, J Hernando-García, T Manzaneque, M Kucera, U Schmid, and J L Sánchez-Rojas. Modelling out-of-plane and in-plane resonant modes of microplates in liquid media. *Journal of Micromechanics and Microengineering*, 25(7):074005, jul 2015.

[60] Gaetan Kerschen. *Modal Analysis of Nonlinear Mechanical Systems*, volume 555 of *CISM International Centre for Mechanical Sciences*. Springer Vienna, Vienna, 1 edition, 2014.

[61] J. P. Noël, Ludovic Renson, Chiara Grappasonni, and Gaëtan Kerschen. Experimental Modal Analysis of Nonlinear Structures Using Broadband Data. In *Nonlinear Dynamics, Volume 1, Conference Proceedings of the Society for Experimental Mechanics Series*, chapter 21, pages 219–240. Springer, 2016.

[62] Rune Brincker and Carlos Ventura. *Introduction to Operational Modal Analysis*. Wiley, 1 edition, 2015.

[63] Firdaus E. Udwadia. A Note on Nonproportional Damping. *Journal of Engineering Mechanics*, 135(11):1248–1256, nov 2009.

[64] O Ozdoganlar, B Hansche, and T Carne. Modal testing techniques for microelectromechanical systems (MEMS). *Proc. 4th International Symposium on MEMS and Nanotechnology*, (January):124–129, 2003.

[65] Min Hu, Jin Xie, Shih-Fu Ling, Hejun Du, and Yongqing Fu. Dynamic testing of micro devices using PZT base excitation. volume 5852, pages 633–638, apr 2005.

[66] X Kang, C J Tay, C Quan, and X Y He. Dynamic characterization of MEMS structures by ultrasonic wave excitation. *Journal of Micromechanics and Microengineering*, 17(12):2426–2431, dec 2007.

[67] O Anac and I Basdogan. Model Validation and Performance Prediction in the Design of Micro Systems. *Journal of Vibration and Control*, 14(11):1711–1728, 2008.

[68] X. Kang, X. Y. He, C. J. Tay, and C. Quan. Non-contact evaluation of the resonant frequency of a microstructure using ultrasonic wave. *Acta Mechanica Sinica*, 26(2):317–323, may 2010.

[69] Daniel Kiracofe and Arvind Raman. On eigenmodes, stiffness, and sensitivity of atomic force microscope cantilevers in air versus liquids. *Journal of Applied Physics*, 107(3):033506, 2010.

[70] Thomas M. Huber, Bradley C. Abell, Daniel C. Mellema, Matthew Spletzer, and Arvind Raman. Mode-selective noncontact excitation of microcantilevers and microcantilever arrays in air using the ultrasound radiation force. *Applied Physics Letters*, 97(21):214101, 2010.

[71] Allyson L. Hartzell, Mark G. da Silva, and Herbert R. Shea. *MEMS Reliability*, volume 1 of *MEMS Reference Shelf*. Springer US, Boston, MA, 2011.

[72] Daniel Kiracofe and Arvind Raman. Quantitative force and dissipation measurements in liquids using piezo-excited atomic force microscopy: a unifying theory. *Nanotechnology*, 22(48):485502, dec 2011.

[73] G. De Pasquale and A. Somà. Dynamic identification of electrostatically actuated MEMS in the frequency domain. *Mechanical Systems and Signal Processing*, 24(6):1621–1633, aug 2010.

[74] Yanghe Shi, Honghai Zhang, Xuefang Wang, and Sheng Liu. A Base Exciter for Dynamic Testing of MEMS on Wafer Level. In *2006 7th International Conference on Electronic Packaging Technology*, number 7, pages 1–3. IEEE, aug 2006.

[75] Murali Krishna Ghatkesar, Thomas Braun, Viola Barwich, Jean-Pierre Ramseyer, Christoph Gerber, Martin Hegner, and Hans Peter Lang. Resonating modes of vibrating microcantilevers in liquid. *Applied Physics Letters*, 92(4):043106, 2008.

[76] Matteo Aureli, Christopher Pagano, and Maurizio Porfiri. Nonlinear finite amplitude torsional vibrations of cantilevers in viscous fluids. *Journal of Applied Physics*, 111(12):124915, 2012.

[77] Santiago D. Solares and Gaurav Chawla. Frequency response of higher cantilever eigenmodes in bimodal and trimodal tapping mode atomic force microscopy. *Measurement Science and Technology*, 21(12):125502, dec 2010.

[78] Elena T. Herruzo and Ricardo Garcia. Frequency response of an atomic force microscope in liquids and air: Magnetic versus acoustic excitation. *Applied Physics Letters*, 91(14):143113, 2007.

[79] Abdelhamid Maali, Cedric Hurth, Rodolphe Boisgard, Cedric Jai, Touria Cohen-Bouhacina, and Jean-Pierre Aime. Hydrodynamics of oscillating atomic force microscopy cantilevers in viscous fluids. *Journal of Applied Physics*, 97(7):074907, 2005.

[80] George Gabriel Stokes. On the Effect of the Internal Friction of Fluids on the Motion of Pendulums. In *Mathematical and Physical Papers vol.1*, volume 9, pages 75–129. Cambridge University Press, Cambridge, 1850.

[81] Arvind Raman and Daniel Kiracofe. Nonlinear dynamics of atomic force microscope microcantilevers in liquid environments - a review. *NOLTA, IEICE*, 4(3):184–197, 2013.

[82] Franz-Josef Elmer and Markus Dreier. Eigenfrequencies of a rectangular atomic force microscope cantilever in a medium. *Journal of Applied Physics*, 81(12):7709, 1997.

[83] Stefan Kirstein, Michael Mertesdorf, and Monika Schonhoff. The influence of a viscous fluid on the vibration dynamics of scanning near-field optical microscopy fiber probes and atomic force microscopy cantilevers. *Journal of Applied Physics*, 84(4):1782, 1998.

[84] Cornelis A. Van Eysden and John E. Sader. Frequency response of cantilever beams immersed in viscous fluids with applications to the atomic force microscope: Arbitrary mode order. *Journal of Applied Physics*, 101(4):044908, 2007.

[85] Sudipta Basak, Arvind Raman, and Suresh V. Garimella. Hydrodynamic loading of microcantilevers vibrating in viscous fluids. *Journal of Applied Physics*, 99(11):114906, 2006.

[86] Alessandro Ricci, Giancarlo Canavese, Ivan Ferrante, Simone Luigi Marasso, and Carlo Ricciardi. A finite element model for the frequency spectrum estimation of a resonating microplate in a microfluidic chamber. *Microfluidics and Nanofluidics*, 15(2):275–284, aug 2013.

[87] M.G. Silk. Modelling of piezoelectric ultrasonic transducers. In *Ultrasonic Transducers for Non Destructive Testing*, chapter 3, pages 25–50. Adam Hilger Ltd, CRC Press, 1984.

[88] M.G. Silk. Variability of piezoelectric transducers. In *Ultrasonic Transducers for Non Destructive Testing*, chapter 6, pages 94–110. Adam Hilger Ltd, CRC Press, 1984.

[89] M.G. Silk. Pulse shape modifications for piezoelectric probes. In *Ultrasonic Transducers for Nondestructive Testing*, chapter 4, pages 51–75. Adam Hilger Ltd, CRC Press, 1984.